A novel human fetal lung-derived alveolar organoid model reveals mechanisms of surfactant protein C maturation relevant to interstitial lung disease

Kyungtae Lim*[,1,2], Eimear N. Rutherford*[,3], Dawei Sun[1,2,4], Dick J. H. Van den Boomen[5,6], James R. Edgar[7], Jae Hak Bang[8], Lydia E. Matesic[9], Joo-Hyeon Lee[2,8], Paul J. Lehner[5], Stefan J. Marciniak[3,10], Emma L. Rawlins[1,2,$] and Jennifer A. Dickens[3,10,$]

* co-first authors

$ co-corresponding authors

1. Wellcome Trust/CRUK Gurdon Institute, University of Cambridge, Cambridge CB2 1QN, UK.

2. Department of Physiology, Development and Neuroscience, University of Cambridge, Cambridge CB2 3DY, UK.

3. Cambridge Institute for Medical Research, Cambridge, CB2 0XY, UK

4. Current address: Broad Institute of Massachusetts Institute of Technology and Harvard, Cambridge, MA 02142, USA.

5. Cambridge Institute of Therapeutic Immunology and Infectious Disease, Jeffrey Cheah Biomedical Centre, University of Cambridge, Cambridge CB2 0AW, UK

6. Harvard Medical School, Department of Cell Biology, Harvard University, LHRRB building, 45 Shattuck Street, Boston MA 02115, USA

7. Department of Pathology, University of Cambridge, Cambridge, CB2 1QP, UK.

8. Wellcome-MRC Cambridge Stem Cell Institute, Jeffrey Cheah Biomedical Centre, University of Cambridge, Puddicombe Way, Cambridge CB2 0AW, UK.

9. Department of Biological Sciences, University of South Carolina, 715 Sumter St., Columbia, SC 29208, USA.

10. Royal Papworth Hospital, Papworth Road, Trumpington, CB2 0AY

Contact: jac72@cam.ac.uk

Key words: stem cell, pulmonary fibrosis, surfactant protein C, E3 ligase, ITCH

Alveolar type 2 (AT2) cells maintain lung health by acting as stem cells and producing pulmonary surfactant[1–3]. AT2 dysfunction underlies many lung diseases including interstitial lung disease (ILD), in which some inherited forms result from mislocalisation of surfactant protein C (SFTPC) variants[4,5]. Disease modelling and dissection of mechanisms remains challenging due to complexities in deriving and maintaining AT2 cells *ex vivo.* Here, we describe the development of expandable adult AT2-like organoids derived from human fetal lung which are phenotypically stable, can differentiate into AT1-like cells and are genetically manipulable. We use these organoids to test key effectors of SFTPC maturation identified in a forward genetic screen including the E3 ligase ITCH, demonstrating that their depletion phenocopies the pathological SFTPC redistribution seen for the SFTPC-I73T variant. In summary, we demonstrate the development of a novel alveolar organoid model and use it to identify effectors of SFTPC maturation necessary for AT2 health.

Despite its role in increasing the stability of pulmonary surfactant, SFTPC is not absolutely required for lung development and surfactant secretion[5]. However, its aberrant handling during intracellular trafficking and maturation results in toxic gain-of-function effects. This is demonstrated by the pathogenic variant I73T, which accumulates immature isoforms at the plasma membrane and causes heritable forms of pulmonary fibrosis[6,7]. Study of this variant in immortalised cells has suggested SFTPC trafficking into multivesicular bodies (MVBs) is indirect (via the plasma membrane) and requires its ubiquitination[8]. Despite the substituted amino acid (I73) lying on the opposite side of the membrane to the ubiquitinated site at K6, failure of ubiquitination appears to be the key determinant of SFTPC-I73T redistribution and the cause of AT2 dysfunction and consequently ILD. Immortalised cells can be used to generate hypotheses, but questions regarding mechanisms and key effectors of SFTPC trafficking can ultimately only be answered using genetically-manipulable physiological AT2 cells which endogenously process surfactant.

58 AT2 organoids have been grown from human adult lungs and used as models of SARS-CoV-2
59 infection[9–11]. Human adult AT2 organoids proliferate slowly and are difficult to genetically
60 manipulate. AT2 organoids can also be derived from pluripotent stem cells (PSC-iAT2s)[12–14]. These
61 cells can readily be genetically manipulated, but their differentiation is complicated, taking more than
62 30 days[15], and PSC-iAT2s can spontaneously dedifferentiate to other organ lineages[14]. AT2 cells have
63 been derived from human fetal lungs, but these cells could neither be genetically manipulated nor
64 maintained long-term in culture[16]. A complementary method for growing genetically-manipulable
65 human AT2 cells would therefore be of great value for investigating surfactant trafficking and lung
66 disease.
67
68 During human lung development the distal tip epithelial cells act as multipotent progenitors[17,18]. From
69 ~15 pcw (post conception weeks) the human tips retain progenitor marker expression, but also
70 upregulate markers of AT2 cells[19]. Immature AT2 cells appear in the tissue from 17 pcw[19,20]. We
71 have recently shown that 16-22 pcw epithelial tip cells can be expanded as organoids and
72 differentiated to AT2 cells[19]. However, the differentiated AT2 organoids were not proliferative,
73 limiting their use for functional studies and genetic manipulation. We have now developed a highly
74 robust, efficient, and scalable culture condition that induces the differentiation of 16-22 pcw fetal
75 lung tip cells into mature AT2 cells which grow as expandable 3D organoids. Here, we characterise
76 the fetal-derived AT2 organoids (hereafter fdAT2), showing that they are stable over long-term
77 passaging, efficiently process and secrete surfactant, and can differentiate into AT1-like cells *in vitro*
78 and in mouse lung transplantation assays. We use a forward genetic screen to identify candidate
79 effectors of SFTPC trafficking which we validate using CRISPR interference (CRISPRi) in the fdAT2
80 organoids. We demonstrate that trafficking of SFTPC requires ubiquitination by HECT domain E3
81 ligases, particularly ITCH, and that their depletion phenocopies the redistribution seen for the
82 pathological SFTPC^{I73T} variant.
83

84 Our AT2 medium directly induces the differentiation of 16-22 pcw fetal lung tip cells into mature
85 AT2 cells which grow as expandable 3D organoids (Fig. 1A; Extended Data Fig. 1A-C). The AT2
86 organoids form within 3 weeks and can be split every week, for over 20 passages, while sustaining
87 *SFTPC* promoter-GFP reporter and AT2 marker expression (Fig. 1B; Extended Data Fig. 1D,E). They
88 retain these characteristics following cryopreservation and thawing. The fetal-derived AT2 (fdAT2)
89 organoids show mature AT2 cell features including, genesis of lamellar bodies and production and
90 secretion of mature forms of SFTPB and SFTPC (Fig. 1C-D; Extended Data Fig. 1F). The organoids
91 express proteins required for surfactant production, such as LAMP3, ABCA3, and NAPSA, as well
92 as typical AT2 markers HTII-280 and HOPX, whereas a fetal tip progenitor marker, SOX9 was not
93 detected (Fig. 1E). Immature SFTPC is detectable at the plasma membrane in these cells, supporting
94 our previous model of SFTPC trafficking (Fig. 3C) in which proprotein transits the cell surface before
95 it is endocytosed and cleaved *en route* to later compartments[8] (Fig. 1F). In addition, the fdAT2
96 organoids expressed cellular polarity markers ZO-1 and laminin, and proliferation marker, Ki67 (Fig.
97 1E). Proliferation of the fdAT2 organoids was greatly reduced when FGF7 was removed from the
98 medium (Extended Data Fig. 1G-I), suggesting that FGF7 is a key mitogen for these cells, consistent
99 with recent mouse data[21]. These culture conditions induce the differentiation of 16-22 pcw lung
100 epithelial progenitors into mature AT2 cells which maintain identity and function during prolonged
101 passaging.
102
103 To further investigate the maturity of fdAT2 organoids, we compared the transcriptome of four
104 independent lines at early passage (fdAT2 early; at P1,4,6,7) and late passage (fdAT2 late; at
105 P12,13,16,17) with those of pluripotent stem cell-derived 3D cultured induced AT2 (PSC-iAT2[12]),
106 freshly-isolated and cultured adult AT2 cells[13] and 8-9 pcw and 16-20 pcw fetal lung tip progenitor
107 organoids[19] (Fig. 1G). Our fdAT2 organoids clustered with other cultured AT2 cells, but were distinct
108 from the fetal lung tip progenitors (PC1, Fig. 1G; Extended Data Fig. 2A). The fdAT2 organoids were
109 transcriptionally closest to the PSC-iAT2 (Fig. 1G). The cultured adult AT2 cells sat between the

110 fdAT2 organoids and the freshly-isolated adult AT2 cells, indicating a culture-effect on the gene
111 expression profile of adult AT2 cells[22] (Fig. 1G). A direct comparison of the fdAT2s and adult
112 cultured AT2s revealed that the most significantly increased transcripts in fdAT2s are related to cell
113 division (Extended Data Fig. 2B), consistent with their expandability. Importantly, the transcriptional
114 profile of the fdAT2 organoids remained stable during the extended culture period, suggesting that
115 expansion of these organoids does not affect AT2 cell identity/function (Fig. 1G; Extended Data Fig.
116 2A,B).
117
118 To further characterise the fdAT2 organoids, we extracted AT2-specific differentially expressed
119 genes (DEGs) by comparing AT2 cells from each source to 16-20 pcw fetal tip progenitor organoids
120 (Fig. 1H; $\log_2$FC>2, *P*-value<0.05). Comparison of these DEGs identified gene expression profiles
121 that distinguish the different AT2 cells. This showed that 51% of DEGs (4,083) are commonly shared
122 across all AT2 cell sources (Fig. 1H; centre). Gene ontology (GO) analysis showed that these genes
123 are related to cytoplasmic translation, protein transport, vesicle-mediated transport, and ER-Golgi
124 vesicle-mediated transport (Extended Data Fig. 2C). Consistent with this, the fdAT2 organoids
125 exhibited a gene expression profile related to surfactant protein synthesis (Fig. 1I). Our DEG analysis
126 also identified subsets of genes that were partially shared, or uniquely expressed, in the different AT2
127 cells (Fig. 1H; Extended Data Fig. 2C). For example, GO analysis for 532 DEGs that are shared by
128 fdAT2 organoids and adult AT2 cells, but not by PSC-iAT2, showed terms associated with vesicle
129 cytoskeletal trafficking, lipid storage, transmembrane transport, and lysosome localization (Fig. 1H,J;
130 Extended Data Fig. 2C'). These GO terms are strongly correlated with the physiological surfactant-
131 producing function of the AT2 cells (Fig. 1D-F) highlighting the utility of the fdAT2 organoids to
132 study surfactant processing. By contrast, the fetal-derived and iPSC-derived AT2 organoids were
133 missing 355 DEGs related to antigen processing and presentation via MHC class II and immune
134 response that only the adult AT2 cells expressed (Fig. 1H,K; Extended Data Fig. 2C''), suggesting
135 that immune function cannot be acquired in a cell-autonomous manner *in vitro*.

136

137 Next, we investigated how far the transcriptional state of the fdAT2 organoids resembles the PSC-
138 iAT2. Their transcriptome is broadly similar (Fig. 1G, Extended data Fig. 2A). However, a direct
139 comparison indicated >2000 DEGs (Extended Data Fig. 2D). Gene set enrichment analysis (GSEA)
140 showed that the fdAT2 organoids were enriched with gene sets associated with surfactant metabolism
141 compared to PSC-iAT2, although they share many pathways (Extended Data Fig. 2E-G). Overall,
142 these data confirm that fdAT2 organoids strongly resemble adult AT2 cells at a transcriptional level
143 and possess the capacity for mature surfactant protein production, trafficking, and secretion, while
144 proliferating. However, the fdAT2 organoids lack immune response-related features. This may reflect
145 some immaturity, or, more likely, the sterile environment in which they are grown; supported by the
146 observation that adult AT2 gradually lose their immune signature when cultured (Fig. 1K, Extended
147 Data Fig. 2A).

148

149 Adult AT2 cells function as facultative progenitors of lung alveoli that can self-renew and
150 differentiate into alveolar type 1 (AT1) cells to replenish AT1 cells upon injury[2,3]. We investigated
151 whether the fdAT2 organoids have the capacity to differentiate into AT1-like cells. The fdAT2
152 organoids were treated with AT1 lineage-promoting conditions: 10% human serum medium on 2D
153 for 2 weeks[10], or 10 mM LATS-IN-1, an inhibitor of LATS1/2 kinases causing activated YAP
154 signalling, in 3D for 1 week[23] (Fig. 2A-G). In both conditions, the fdAT2 organoids showed
155 upregulation of AT1 fate markers, such as *AQP5*, *CAV1*, and *AGER*, and downregulation of *SFTPC*
156 and *SFTPC*-GFP (Fig. 2C,D,F,G). Next, we tested whether the fdAT2 organoids could differentiate
157 in a more physiological environment. We dissected adult mouse lungs and injected them with single-
158 cells isolated from *SFTPC*-GFP;*EF1a*-RFP-expressing human fdAT2 organoids, followed by
159 precision-cut lung slice (PCLS) culture for 1 week. The RFP^+ human cells were engrafted into the
160 alveolar structure in the mouse PCLS and showed flattened nuclei, consistent with reports that AT1
161 cells have flattened nuclear shape[24] (Fig. 2I-J; Supplementary Video 1). Scoring for the *SFTPC*-GFP

162 reporter and AT1/2 fate markers confirmed that nearly 100% of the RFP$^+$ cells co-expressed the AT1
163 lineage markers, CAV1 and AGER, and rarely expressed the *SFTPC*-GFP reporter or SFTPC protein
164 (Fig. 2H-K). Taken together, these data show that the human fdAT2 organoids are competent to
165 differentiate to the AT1 cell lineage *in vitro* and in the mouse lung environment *ex vivo*.
166
167 Our data indicate that the fdAT2 organoids self-renew, differentiate to AT1 cells and display a mature
168 surfactant synthesis profile during prolonged passaging. They are amenable to lentiviral transduction
169 and therefore represent a physiological system to study mechanisms of fundamental AT2 function
170 and dysfunction in disease.
171
172 The commonest pathogenic variant of SFTPC, I73T, mislocalises to the plasma membrane and causes
173 AT2 dysfunction via a toxic gain-of-function effect leading to ILD[6,7]. We were able to reproduce this
174 cell surface phenotype in the fdAT2 organoids by viral transduction of HA-SFTPC variants (Fig.
175 3A,B). Ubiquitinated SFTPC is recognised by the ESCRT machinery and trafficked to late
176 compartments. We previously showed that the disease-causing SFTPC-I73T mutant is no longer
177 ubiquitinated, resulting in its relocalisation via recycling and saturated endocytosis of immature
178 isoforms[8] (Fig. 3C). To identify the ubiquitination machinery required for ESCRT recognition of
179 SFTPC, we performed a targeted forward genetic screen (Fig. 3D). We predicted that depletion of
180 key effectors of SFTPC ubiquitination would phenocopy the I73T variant by causing SFTPC
181 accumulation at the plasma membrane. HeLa cells stably expressing GFP-SFTPC and Cas-9 were
182 transduced with a subgenomic ubiquitome sgRNA library[25], and cells with increased surface-
183 localised pro-SFTPC when compared with untransduced controls were harvested at day 7 or 14
184 (Extended Data Fig. 3A,B). Transduced cells were also sorted for total SFTPC (GFP-high) to ensure
185 that any cells accumulating C-terminally cleaved SFTPC at the cell surface (and thus missing the
186 antibody epitope) were not overlooked (Extended Data Fig 3C,D).
187

188 The most enriched gRNA in d7 cell surface SFTPC-high cells targeted Itchy E3 Ubiquitin Protein
189 Ligase (*ITCH)* (Fig. 3E; Extended Data Fig. 3A; Extended Data Table 4). Guide RNAs targeting the
190 ESCRT machinery components Hepatocyte Growth Factor-Regulated Tyrosine Kinase Substrate
191 (*HRS)* and VPS28 Subunit of ESCRT-I (*VPS28),* K63-chain specific Ubiquitin E2 Conjugating
192 Enzyme E2 N (*UBE2N)* and the early endosome Rab5-specific GEF RAB Guanine Nucleotide
193 Exchange Factor 1 (*RABGEF1)* were also enriched; supporting our previous data that SFTPC transits
194 early endosomal compartments before K63-ubiquitination, recognition by the ESCRT complex and
195 transit into MVBs. These hits largely overlapped with the GFP-defined sort which also included
196 gRNAs targeting *ITCH* and ESCRT machinery (Extended Data Fig. 3C). Enrichment of gRNAs for
197 sumoylation-related Ubiquitin Conjugating Enzyme E2 I (*UBE2I)*, Ubiquitin Like Modifier
198 Activating Enzyme 2 (*UBA2)* and Protein Inhibitor Of Activated STAT 1 (*PIAS1)* was noted in both
199 screens. *ITCH* remained highly enriched in the d14 sort, though other specific hits (e.g. *HRS*, *VSP28*,
200 *UBE2N*) were lost likely due to their fundamental roles in trafficking and thus cellular toxicity when
201 depleted (Extended Data Fig. 3A,B).
202
203 Initial validation of *ITCH*, SUMOylation components and positive controls *HRS* and *UBE2N*
204 (Extended Data Fig. 4A) revealed that individual depletion resulted in marked cell surface GFP-
205 SFTPC localisation (Extended Data Fig. 4B). Enrichment of full length SFTPC was more modest
206 (Extended Data Fig 4C,D), suggesting that a proportion of surface-localised SFTPC is C-terminally
207 cleaved. We used RT-qPCR to test the hypothesis that SUMOylation hits reflected changes in global
208 transcription[26], rather than SFTPC trafficking (Extended Data Fig. 4E) and based on these data
209 SUMOylation was not investigated further.
210
211 ITCH is a HECT-type E3 ligase whose WW domains recognise cytosolic proline rich consensus
212 sequences, typically PPxY which is present within the N-terminal tail of SFTPC[27]. Depletion of *ITCH*
213 in clonal GFP-SFTPC expressing HeLa lines did not affect *SFTPC* transcription (Fig. 3F, I), but

214 markedly increased plasma membrane resident SFTPC (Fig. 3G, H, J). Immunoblotting revealed an
215 excess of full-length (*), partially cleaved (**) and fully C-terminally cleaved (***) species,
216 suggesting that ITCH depletion inhibits trafficking at/beyond the location of the final C-terminal
217 cleavage which is thought to be at the MVB limiting membrane[8,28] (Fig. 3I). We confirmed that
218 SFTPC resides largely in LAMP3^{+} (late) compartments in control cells. Following ITCH depletion,
219 SFTPC relocalised to EEA1^{+} early endosomes and MICALL1^{+} recycling endosomes, consistent with
220 failure of MVB entry and recycling to the plasma membrane (Fig. 3J). In rescue experiments,
221 restoration of ITCH in knockout cells reversed SFTPC mislocalisation (Extended Data Fig. 5). These
222 data suggest that ITCH is required for SFTPC trafficking and that ITCH depletion causes
223 relocalisation of SFTPC to the plasma membrane, phenocopying SFTPC-I73T.
224
225 Having identified ITCH as an E3 ligase required for SFTPC maturation using HeLa cells, we wanted
226 to determine whether ITCH also regulated endogenous SFTPC trafficking in primary AT2 cells. We
227 therefore used CRISPRi to genetically deplete fdAT2 organoids of ITCH and UBE2N, as well as the
228 HECT domain E3 ligase, NEDD4-2, which has been reported to play a role in SFTPC ubiquitination
229 and maturation[29,30]. *NEDD4-2* was not isolated in our screen likely due to its relative lack of
230 expression in HeLa (~20% that of *ITCH;* **www.ebi.ac.uk/gxa**), but it is expressed in fdAT2 at a
231 similar level to *ITCH* (Extended Data Fig. 2H).
232
233 CRISPRi-expressing fdAT2 organoids were transduced with a gRNA for each gene and silencing
234 induced[31] (Fig. 4A). Approximately 50% of organoids expressed both the CRISPRi and gRNA after
235 5 days of induction (Fig. 4B and Extended Data Fig. 6A,B). The toxicity of silencing ubiquitin ligases
236 precluded sorting the double-positive population for RNA extraction, so the 40-60% overall gene
237 depletion likely reflects complete gene depletion in dual-positive organoids (Fig. 4C). The knock-
238 down effects reversed completely if organoids were recovered without silencing (-TMP/-dox) (Fig.
239 4D,E bottom panel 'recovery').

240

241 Global inhibition of K63-ubiquitination and more targeted inhibition of ubiquitination (via *UBE2N*
242 or *NEDD4-2* depletion respectively) resulted in massive accumulation of intracellular SFTPC with
243 partial relocalisation to the plasma membrane (Fig. 4E top and middle rows). *ITCH* depletion resulted
244 in a similar, but exaggerated, phenotype to that of *NEDD4-2* depletion, and dual-knockdown further
245 exacerbated the intracellular and cell surface SFTPC accumulation. The cell surface relocalisation
246 likely reflects both active recycling of C-terminally cleaved protein and an excess of full-length
247 protein, which is detectable by flow cytometry (Fig. 4F and Extended Data Fig. 6C). Depletion of
248 SFTPC ubiquitin ligases in human fdAT2 organoids results in mislocalisation of the endogenous
249 SFTPC.

250

251 ITCH deficiency causes lung interstitial inflammatory infiltrates in humans and mouse models[32,33]
252 thought to result from multisystem autoimmune disease. We predicted an additional alveolar
253 epithelial phenotype if ITCH is important for SFTPC maturation *in vivo.* Staining for pro-SFTPC
254 revealed intracellular accumulation and an altered distribution in *Itch* deficient ($Itch^{a18H/a18H}$) mouse
255 alveolar epithelium. Numerous, smaller pro-SFTPC puncta are consistent with failure of trafficking
256 to late compartments, seen as large puncta in the wild-type mice (Fig. 4G).

257

258 We conclude that intracellular trafficking of SFTPC requires K63 ubiquitination mediated by the
259 HECT domain E3 ligases including ITCH and, to a lesser extent, NEDD4-2. Inhibiting ubiquitination
260 phenocopies the redistribution of the pathogenic SFTPC-I73T variant, reinforcing the importance of
261 this post-translational modification in maintaining AT2 health.

262 We have derived an expandable AT2 organoid model from fetal lung tip progenitor cells and
263 demonstrated its use in investigating mechanisms of AT2 biology relevant to disease. FdAT2
264 organoids acquire features of mature adult AT2 cells, including lamellar body formation, mature
265 surfactant protein secretion, and the ability to differentiate to AT1 cells (Figs. 1,2). In contrast to
266 human adult lung-derived AT2 organoids[9–11], the fdAT2 organoids readily expand, can be passaged
267 multiple times and cryopreserved without compromising their identity. Their transcriptome is similar
268 to that of PSC-iAT2 (Fig. 1G), but they can be derived in a more straightforward and timely fashion.
269 They are also amenable to genetic manipulation, enabling us to investigate key SFTPC trafficking
270 effectors using CRISPRi (Figs. 3,4).
271
272 Complete trafficking and maturation of SFTPC is required for AT2 health; misfolding variants are
273 retained in early compartments and cause ER stress[34,35] whereas mistrafficking isoforms, exemplified
274 by SFTPC-I73T, mislocalise due to a trafficking block and failure of ubiquitination[8,35,36]. Both
275 mutation types result in AT2 cell dysfunction and heritable forms of interstitial lung disease. These
276 phenotypes have been confirmed in animal models[37–39], but mechanistic work on AT2 dysfunction in
277 physiological human *ex vivo* models has been highly challenging. We combined a forward genetic
278 screen with genetic manipulation of fdAT2 organoids to investigate intracellular SFTPC trafficking
279 via the plasma membrane (Fig. 1D). We confirm that ubiquitination is required for normal SFTPC
280 trafficking and identify the E3 ligase ITCH as a novel effector of SFTPC processing. Although there
281 can be redundancy between family members, the observation that individual depletion of either ITCH
282 or NEDD4-2 (expressed at similar levels in human AT2 cells) yields a phenotype close to that of dual
283 depletion (Fig. 4E) suggests they may play complementary roles. We further confirmed altered
284 SFTPC handling in *Itch* deficient mice (fig 4G).
285
286 FdAT2 organoids are an attractive genetic model for understanding fundamental mechanisms of AT2
287 cell biology in health, and modelling inherited disorders and environmental insults which perturb

288 their function. They also represent a useful cell source to investigate cellular and molecular
289 mechanisms of AT2 to AT1 cell lineage differentiation during human lung development and repair.
290

291 **Acknowledgements**

292 We would like to acknowledge the imaging facilities at the Gurdon Institute and Cambridge Institute
293 for Medical Research and the flow cytometry facility at the Cambridge Institute for Medical Research
294 (CIMR).
295

296 KL is supported by the Basic Science Research Program through the National Research Foundation
297 of Korea (NRF) funded by the Ministry of Education (2018R1A6A3A03012122). ENR and JAD are
298 supported by an MRC Clinician Scientist Fellowship (MR/S005552/1). DS is supported by a
299 Wellcome Trust PhD studentship (109146/Z/15/Z) and the Department of Pathology, University of
300 Cambridge. JRE is supported by a Sir Henry Dale Fellowship jointly funded by the Wellcome Trust
301 and the Royal Society (216370/Z/19/Z). LEM was supported in part by the National Institute of
302 General Medical Sciences of the National Institutes of Health under Award Number P20GM103499.
303 J-HL and JHB are supported by a Wellcome Senior Research Fellowship (221857/Z/20/Z) and the
304 Suh Kyungbae Foundation (SUHF-20010033). SJM is supported by the MRC (MCMB
305 MR/V028669/1 and MR/R009120/1), EPSRC (EP/R03558X/1), Cambridge Biomedical Research
306 Centre (BRC-1215-20014); Asthma+Lung UK (ALUK), and the Victor Philip Dahdaleh Foundation.
307 ELR is supported by the Medical Research Council (MR/P009581/1). PJL and DJHVB are supported
308 by a Wellcome Trust Principal Research Fellowship (210688/Z/18/Z) and an MRC project grant
309 (MR/V011561/1).
310

311 We acknowledge core funding to the Gurdon Institute from the Wellcome Trust (203144/Z/16/Z) and
312 CRUK (C6946/A24843). This research was also supported by the CIMR Flow Cytometry Core
313 Facility.

Author contributions

Conceptualisation, KL, ENR, PJL, SJM, ELR, JAD; Methodology, Investigation, and Validation, KL, ENR, DS, DJHVB, JRE, LEM, JAD; Resources, LEM, PJL; Software and Formal Analysis, KL, ENR, DJHVB; Writing – Original Draft KL, ENR; Writing – Review & Editing, JHL, PJL, SJM, ELR, JAD; Funding Acquisition and Supervision: JHL, PJL, SJM, ELR, JAD.

323 **Figure legends**

324

325 **Fig. 1. Human fetal-derived alveolar type 2 organoids show similar surfactant protein**
326 **production, trafficking, and secretion to adult AT2 cells.** (A) Experimental scheme and culture
327 medium for derivation and establishment of fdAT2 organoids from human fetal lungs at 16-22 pcw.
328 (B) Bright-field images of two independent fdAT2 organoid lines at P3, which were established from
329 19 pcw fetal lung tissue. (C) Uptake of lysotracker green DND-26 that stains acidic compartments
330 within an fdAT2 organoid line at P14, showing the accumulation of lamellar bodies (acidic lysosome-
331 related organelles). (D) Electron microscopy showing the presence of lamellar bodies with
332 characteristic concentric lamellar membranes. Scale bar, 2 μm. (E) Immunofluorescence images of
333 fdAT2 organoids using surfactant protein production-associated markers including mature SFTPC
334 and SFTPB, LAMP3, NAPSA, and ABCA3, plus typical alveolar type 2 cell-lineage markers HTII-
335 280 and HOPX, epithelial cell polarity markers E-cadherin, pan-Laminin, and ZO1, and a
336 proliferation marker, KI67. *Asterisk (yellow) indicates apical lumen. Organoids were at p10-15.
337 DAPI (blue), nuclei. Scale bars, 50 μm. (F) Flow cytometric analysis of cell surface proSFTPC in 9
338 pcw lung tip progenitor organoids and 21 pcw fdAT2 organoids as measured by C-terminal SFTPC
339 antibody which recognises the full-length protein. (G) Principal component analysis (PCA) plot of
340 transcriptomic profiles of the fdAT2 organoids at early and late passages (fdAT2; Early and Late),
341 lung tip progenitor organoids from 7-9 pcw and 16-22 pcw, and other alveolar type 2 cells that were
342 previously reported, PSC-iAT2, adult AT2 cells cultured or freshly isolated from adult human lung[2,3].
343 (H) Venn diagram illustrating the number and the proportion of unique or shared genes from AT2
344 cells of different sources. The genes for each AT2 cell type that were differentially expressed
345 compared to fetal 16-22 pcw tip progenitor organoids were included ($\log_2$FC > 2, *P*-value < 0.05;
346 Extended Data Table 2). (I-K) Heatmap of DEGs associated with typical AT2 cell fate (I), trafficking
347 (J), and immune response (K). A list of trafficking-related genes was selectively obtained following

348 gene ontology (GO) analysis for the GO terms; lipid storage, membrane transport, lysosome
349 localisation, vesicle-cytoskeleton trafficking; see also Extended Data Fig. 2C.
350
351 **Fig. 2. Alveolar type 1 cell fate differentiation of AT2 organoids under *in vitro* and *ex vivo***
352 **culture conditions.** (A-D) Alveolar type 1 cell (AT1) fate differentiation of fdAT2 organoids in 10%
353 human serum-containing medium on 2D culture. Experimental scheme of AT1 differentiation (A), a
354 bright-field image of AT2 organoids upon AT1 differentiation (B), qRT-PCR analysis of AT1
355 markers *AQP5*, *CAV1*, and *AGER*, and an AT2 marker, *SFTPC* (C), and immunofluorescence
356 imaging with CAV1, E-cadherin, β-actin, and DAPI (nuclei) (D). For RT-qPCT, data were
357 normalised to fdAT2 organoids; mean ± SD, n = 3 independent repeats (*p<0.05, **p<0.01; unpaired
358 t-test (two-tailed)). (E-G) AT1 differentiation of *SFTPC*-GFP-expressing fdAT2 organoids in a
359 culture medium containing YAP signalling agonist, 10 μM LATS-IN-1, in the absence of Wnt
360 agonists, in 3D organoid culture. Experimental scheme of AT1 differentiation (E), qRT-PCR analysis
361 of AT1 markers *AQP5*, *CAV1*, and *AGER*, and an AT2 marker, *SFTPC* (F), and immunofluorescence
362 imaging with CAV1, AGER, and DAPI (nuclei) (G). For RT-qPCR, data were normalised to fdAT2
363 organoids; mean ± SD, n=3 independent repeats (*p<0.05, **p<0.01; unpaired t-test (two-tailed)).
364 (H) Explant culture of mouse precision-cut lung slices (PCLS) upon injecting *SFTPC*-GFP; *EF1a*-
365 RFP human fdAT2 organoids. Organoids were dissociated and 2 x 10^5 single cells mixed with 100 μl
366 of 50% matrigel and directly injected into each lobe of the lungs. PCLS of 150 μm thickness were
367 cultured for 1 week in 10% fetal bovine serum-containing medium. Three independent lines of fdAT2
368 organoids were used for the explant culture (16402, 16587, 16392). (I-K) Immunofluorescence
369 images of PCLS showing engrafted and AT1 differentiated human cells. RFP+ cells were monitored
370 by a combination of cell type marker antibodies against SFTPC (I,J), and CAV1 (I) or AGER (J).
371 DAPI, nuclei. Scale bars, 50 μm. Quantitation (K) of AT1-lineage positive human cells in the
372 explants, by measuring the proportion of AT2 (SFTPC) and AT1 markers (CAV1 and AGER) co-

373 localising with RFP (n = 53, SFTPC/CAV1 cells; n = 56, SFTPC/AGER cells; 6 lung slices from 3
374 biological replicates).
375
376 **Fig. 3: A forward genetic screen confirms the importance of ubiquitination in SFTPC**
377 **trafficking and identifies the E3 ligase ITCH as required for SFTPC maturation.** (A)
378 Immunofluorescence of proSFTPC localisation in organoids expressing HA-SFTPC-WT or HA-
379 SFTPC-I73T for 10 days. Scale bar 10 µm / 5 µm in zoomed inserts. (B) Quantification of cell surface
380 SFTPC in organoids expressing HA-SFTPC-WT or HA-SFTPC-I73T as measured by SFTPC C-
381 terminal antibody, expressed as fold change in mean fluorescence intensity; mean ± SEM, n=3
382 independent repeats (* = $p<0.05$, one-sample t-test). (C) Schematic of WT and pathogenic I73T
383 variant SFTPC trafficking. After trafficking from early compartments to the plasma membrane, both
384 WT and I73T are endocytosed and the C terminus cleaved in early endosomes. Onward trafficking
385 into multivesicular bodies (MVBs) then lamellar bodies (LBs) is dependent upon further cleavage
386 and ubiquitination; this fails in the I73T variant and results in recycling of partially cleaved isoforms
387 to the plasma membrane. (D) Schematic of ubiquitome forward genetic screen strategy. HeLa cells
388 stably expressing eGFP-SFTPC-WT and Cas9 were infected with a lentiviral ubiquitome sgRNA
389 library consisting of 1,119 genes with 10 guides per gene. Transduced cells were selected with
390 puromycin to generate a mutant cell pool. Day 7 post transduction, cells enriched for cell surface pro-
391 SFTPC (as measured by a C-terminal antibody) or total GFP were isolated by FACS. These cells
392 underwent a further enrichment sort at day 14. Genomic DNA was extracted from sorted cells and an
393 unsorted control and genes with the highest gRNA representation identified by high-throughput
394 sequencing. (E) MAGeCK score demonstrating relative enrichment of each gene for the day 7 cell
395 surface SFTPC high population. (F) Relative expression of *SFTPC* and *ITCH* in control and ITCH
396 knockout (KO) HeLa cells as measured by RT-qPCR and normalised to GAPDH; mean ± SEM, n=3
397 independent repeats (***=$p<0.001$, two-sided student's t-test with non-equal variance). (G, H) Flow
398 cytometry of cell surface SFTPC signal as measured by SFTPC C-terminal (C-term) antibody in

399 control vs ITCH knockout lines and quantification of mean fluorescence intensity; mean ± SEM,
400 n=10 independent repeats (*** = p<0.001, one-sample t-test). (I) Immunoblotting of lysates from
401 control or ITCH knockout cells using an SFTPC N-terminal (Npro) and ITCH antibody (* = full
402 length species (-/+ palmitoylation), ** = partially C-terminal cleaved intermediate, *** = fully C-
403 terminally cleaved intermediate). (J) Live cell imaging and colocalisation of GFP-SFTPC with
404 LAMP3, MICAL-L1 and EEA1 by immunofluorescence in control and ITCH knockout cells. Scale
405 bar, 10 µm.
406
407 **Fig. 4: ITCH depletion alters SFTPC localisation in fetal lung-derived AT2 organoids.** (A)
408 Schematic of the inducible CRISPR interference (CRISPRi) system in fdAT2 organoids. CRISPRi
409 organoid lines were generated by lentiviral transduction of AT2 cells with KRAB-dCas9-DHFR
410 followed by sorting for RFP-positive cells. Cells were replated and expanded for 12 days before
411 transduction with relevant sgRNA lentivirus. Approximately 10 days later the CRISPRi system was
412 activated with doxycycline (dox) and trimethoprim (TMP). 5 days after induction, organoids were
413 analysed by qPCR, flow cytometry and confocal microscopy. Dox and TMP were subsequently
414 removed for 14 days to allow for recovery of gene expression. (B) Representative images showing
415 morphology of control organoids and those transduced with KRAB-dCas9-DHFR (RFP) -/+ gRNA
416 (GFP). Scale bar = 400 µm (C-D) Relative expression of *UBE2N, ITCH,* and *NEDD4-2* following
417 CRISPRi induction (C) and 14-day recovery (D) (representative data from 3 (*ITCH/UBE2N*) or 1
418 (*NEDD4-2*) experiments, each performed in triplicate). Expression level was normalised to organoids
419 expressing non-targeting control gRNAs. (E) proSFTPC localisation in CRISPRi-depleted
420 (knockdown; kd) and recovered organoids by immunofluorescence (top panels: equal microscope
421 settings illustrate accumulation of pro-SFTPC protein; middle panels: exposure altered to visualise
422 subcellular localisation). Scale bar = 10 µm / 5 µm zoomed inserts. (F) Quantification of cell surface
423 SFTPC signal measured by flow cytometry using SFTPC C-terminal antibody, expressed as fold

424 change in mean fluorescence intensity. (G) Intracellular localisation of SFTPC in wild-type or Itch
425 knockout mice.
426
427 **Extended Data Fig. 1. Characterization of AT2 organoids.** (A) Derivation and establishment of
428 fdAT2 organoids from lung tip progenitor cells (upper panel), or proximal airway progenitors (lower
429 panel) of human fetal lungs at 22 pcw. Upper panel: The isolated tip progenitor cells were
430 immediately transduced and selected based on *SFTPC*-GFP and EF1a-TagRFP after 48 h of
431 transduction; *SFTPC*-GFP and EF1a-TagRFP reporter positive cells were efficiently expanded into
432 fdAT2 organoids when grown in AT2 medium for 3 weeks. Lower panel: Proximal airway cells were
433 immediately transduced with *SCGB3A2*-GFP, EF1a-TagRFP reporter lentivirus and the airway
434 progenitor cells were selectively isolated by *SCGB3A2*-GFP after 48h of transduction; *SCGB3A2*-
435 GFP, *EF1a*-TagRFP reporter positive cells and expanded into small AT2-like organoids when grown
436 in AT2 medium for 3 weeks, but efficiently formed airway organoids when grown in airway medium
437 for the same period. Scale bar, 50 µm (B) Size of organoids expanded from tip progenitors (*SFTPC*-
438 GFP^{+}) or proximal airway progenitors (*SCGB3A2*-GFP^{+}) in AT2 medium was measured; mean ± SD,
439 n=50 (****p<0.0001; unpaired t-test (two-tailed)). (C) Expression of mature SFTPC protein in
440 organoids expanded from tip progenitors or airway progenitors in AT2 medium. DAPI, nuclei. Scale
441 bar, 50 µm. (D) Cultured fdAT2 organoids at early and late passages, stably expressing *SFTPC*
442 promoter-driven GFP (*SFTPC*-GFP). Two independent lines of AT2 organoids at P3 and P17, and
443 P4 and P20. Scale bars, 50 µm. (E) qRT-PCR analysis of alveolar type 2 cell lineage markers,
444 *NKX2*.1, *SFTPC*, *ABCA3*, and *LAMP3*, in 7-9 pcw and 16-22 pcw tip progenitor organoids, and
445 fdAT2 organoids at P12, P20, and P21. Data were normalised to 7-9 pcw tip organoids; mean ± SD,
446 n=3 independent repeats (*p<0.05, **p<0.01, ***p<0.001; One-way ANOVA with Tukey multiple
447 comparison post-test). (F) Immunoblot of mature forms of SFTPC and SFTPB in human fetal lung
448 tip progenitor-derived organoids at 7-9 pcw and 16-22 pcw, respectively, and the fdAT2 organoids.
449 Two independent replicates were used. (G - I) FdAT2 organoids were cultured in the AT2 medium

450 for 2 weeks, in the presence (control) or absence of FGF7 (-FGF7) and AT2 lineage markers were
451 measured by qRT-PCR (H) after 7 and 14 days of culture. Data were normalised to AT2 organoids
452 cultured in the AT2 medium containing FGF7 (control); mean ± SD, n=3 independent repeats (*p <
453 0.05, **p < 0.01, ***p < 0.001; one-way ANOVA with Tukey multiple comparison post-test). (I)
454 Mature SFTPC protein expression was visualised with a proliferation marker, KI67, and E-cadherin
455 by immunofluorescence staining, at 14 days of culture. DAPI, nuclei. Scale bar, 50 μm.
456
457 **Extended Data Fig. 2. Comparative transcriptomic analysis of fetal-derived AT2 organoids**
458 **with other AT2 sources.** (A) Heatmap analysis of the top 2,000 most variable genes across all
459 samples. (B) GO analysis of genes highly enriched in the fdAT2 organoids compared to the cultured
460 adult AT2 cells. (C, blue) GO analysis of DEGs shared between AT2 cells of different origin,
461 including fdAT2 organoids, PSC-iAT2, and cultured and freshly isolated adult AT2 cells; related to
462 Fig. 1H. 4,083 genes commonly shared by all AT2 fate cell types. (C', red) genes shared by fdAT2
463 organoids and cultured and/or freshly isolated adult AT2 cells (C''; cyan) genes shared by cultured
464 and freshly isolated adult AT2 cells. (D) Volcano plot describing the direct comparison of fdAT2
465 organoids and PSC-iAT2. 1,855 and 832 genes were differentially enriched in AT2 organoids and
466 PSC-iAT2, respectively (logFC > 2, *P*-value < 0.05; related to Extended Data Table 3). (E and F)
467 Gene set enrichment analysis (GSEA) of surfactant metabolism and signalling pathway-associated
468 gene sets between fdAT2 organoids and PSC-iAT2. (G) Heatmap of a gene set associated with
469 surfactant metabolism from REACTOME. Green box, fdAT2 organoids. (H) Relative expression of
470 E3 ligases *ITCH* and *NEDD4-2* in AT2 cells and tip progenitor organoids. .
471
472 **Extended Data Fig. 3. A forward genetic screen identifies candidate proteins involved in SFTPC**
473 **processing and trafficking.** (A-B) Flow cytometry gating strategy and MAGeCK relative
474 enrichment scores for genes whose depletion results in increased cell surface SFTPC (A, day 7 and
475 B, day 14) or increased total eGFP-SFTPC (C, day 7 and D, day 14) post-transduction with

476 ubiquitome sgRNA library. Genes highlighted red (BAP1,TRIM33 and PHF10) are commonly
477 enriched but non-specific transcription-related hits from forward genetic screens.
478
479 **Extended Data Fig. 4. Initial validation of screen hits.** (A) Schematic of screen hit validation
480 strategy. HeLa cells stably expressing GFP-SFTPC-WT and Cas9 were transfected with plasmids
481 containing sgRNAs against specific genes for hit validation. Three guides for each gene were pooled
482 for transfection. Cells underwent puromycin selection for 48 hours to select for transfected cells. (B-
483 C) Knockout pools assessed for cell surface SFTPC enrichment by live cell confocal microscopy (B)
484 and flow cytometry (C). Scale bar = 10 µm. (D) Quantification of full-length cell surface SFTPC as
485 measured by C-terminal antibody and expressed as mean fluorescence intensity. Mean ± SEM, n=3
486 independent repeats (*$p < 0.05$, **$p < 0.01$,***$p<0.001$; paired two-tailed Student's *t*-test). (E)
487 Relative expression of *SFTPC* mRNA in GFP-SFTPC-Cas9 control cells and UBE2I, UBA2, and
488 PIAS1 knockout pools (representative result of 3 independent repeats).
489
490 **Extended Data Fig. 5. Restoration of ITCH expression in knockout cells reverses SFTPC**
491 **mislocalisation**. Control and ITCH knockout HeLa cells transfected with *HA-ITCH* were assessed
492 for relative *ITCH* mRNA expression (A), GFP-SFTPC localisation (B) and cell surface full-length
493 SFTPC protein by flow cytometry (C&D). Scale bar = 10 µm. Mean ± SEM, n=3 independent repeats
494 (**=$p<0.005$, one-way ANOVA with *post-hoc* Tukey tests).
495
496 **Extended Data Fig. 6. Flow cytometry gating strategy and cell-surface SFTPC measured during**
497 **CRISPRi knockdown and recovery.** (A) Flow cytometry dot plots of sgRNA positive (y-axis) and
498 CRISPRi-RFP (x-axis) positive populations in organoids transduced with sg non-targeting (NT),
499 sgUBE2N, sgITCH, or sgNEDD4-2 at cell harvesting (5 days post induction of CRISPRi system).
500 (B) (top panel) Flow cytometry dot plots of sgRNA positive (y-axis) and CRISPRi-RFP (x-axis)
501 positive populations for cells transduced with both sgITCH and sgNEDD4-2 (5 days post induction

502 of CRISPRi system). The population was first gated for GFP and RFP positive cells. The resulting
503 population (outlined) was gated for BFP positive cells (bottom panel). (C) Flow cytometry of cell
504 surface SFTPC as measured by C-terminal antibody (detecting full length protein) during knockdown
505 (kd) and following rescue when compared with organoids expressing non-targeting control gRNAs.
506
507 **Extended Data Table 1. Multiple comparison of transcriptomes of alveolar type 2 cells of**
508 **different origins.** Transcriptional comparison between fdAT2 organoids with other AT2 cells.
509
510 **Extended Data Table 2. Transcriptomic comparison of AT2 cells compared to those of fetal 16-**
511 **22 pcw tip progenitor organoids.** The genes for each cell type were differentially extracted from
512 those of fetal late tip progenitor organoids (logFC > 2, *P*-value < 0.05).
513
514 **Extended Data Table 3. Direct comparison of transcriptomes of fetal-derived AT2 organoids**
515 **and PSC-iAT2.** Transcriptional comparison between fdAT2 organoids with PSC-iAT2.
516
517 **Extended Data Table 4.** Full list of enriched genes in ubiquitome forward genetic screens at day 7
518 and day 14.
519
520

521 **References**

522

523 1. Zepp, J. A. & Morrisey, E. E. Cellular crosstalk in the development and regeneration of the
524 respiratory system. *Nat. Rev. Mol. Cell Biol.* **20**, 551–566 (2019).

525 2. Desai, T. J., Brownfield, D. G. & Krasnow, M. A. Alveolar progenitor and stem cells in lung
526 development, renewal and cancer. *Nature* **507**, 190–194 (2014).

527 3. Barkauskas, C. E. *et al.* Type 2 alveolar cells are stem cells in adult lung. *J. Clin. Invest.* **123**,
528 3025–3036 (2013).

529 4. Parimon, T., Yao, C., Stripp, B. R., Noble, P. W. & Chen, P. Alveolar Epithelial Type II Cells
530 as Drivers of Lung Fibrosis in Idiopathic Pulmonary Fibrosis. *Int. J. Mol. Sci.* **21**, (2020).

531 5. Glasser, S. W. *et al.* Altered stability of pulmonary surfactant in SP-C-deficient mice. *Proc. Natl.*
532 *Acad. Sci. U. S. A.* **98**, 6366–6371 (2001).

533 6. Brasch, F. *et al.* Interstitial lung disease in a baby with a de novo mutation in the SFTPC gene.
534 *Eur. Respir. J.* **24**, 30–39 (2004).

535 7. Alysandratos, K.-D. *et al.* Patient-specific iPSCs carrying an SFTPC mutation reveal the
536 intrinsic alveolar epithelial dysfunction at the inception of interstitial lung disease. *Cell Rep.* **36**,
537 109636 (2021).

538 8. Dickens, J. A. *et al.* Novel insights into surfactant protein C trafficking revealed through the
539 study of a pathogenic mutant. *Eur. Respir. J.* **59**, (2022).

540 9. Youk, J. *et al.* Three-Dimensional Human Alveolar Stem Cell Culture Models Reveal Infection
541 Response to SARS-CoV-2. *Cell Stem Cell* **27**, 905-919.e10 (2020).

542 10. Katsura, H. *et al.* Human Lung Stem Cell-Based Alveolospheres Provide Insights into SARS-
543 CoV-2-Mediated Interferon Responses and Pneumocyte Dysfunction. *Cell Stem Cell* **27**, 890-
544 904.e8 (2020).

545 11. Salahudeen, A. A. *et al.* Progenitor identification and SARS-CoV-2 infection in human distal
546 lung organoids. *Nature* **588**, 670–675 (2020).

547 12. Jacob, A. *et al.* Differentiation of Human Pluripotent Stem Cells into Functional Lung Alveolar
548 Epithelial Cells. *Cell Stem Cell* **21**, 472-488.e10 (2017).
549 13. Abo, K. M. *et al.* Air-liquid interface culture promotes maturation and allows environmental
550 exposure of pluripotent stem cell-derived alveolar epithelium. *JCI Insight* **7**, (2022).
551 14. McCauley, K. B. *et al.* Single-Cell Transcriptomic Profiling of Pluripotent Stem Cell-Derived
552 SCGB3A2+ Airway Epithelium. *Stem Cell Reports* **10**, 1579–1595 (2018).
553 15. Jacob, A. *et al.* Derivation of self-renewing lung alveolar epithelial type II cells from human
554 pluripotent stem cells. *Nat. Protoc.* **14**, 3303–3332 (2019).
555 16. Gonzales, L. W., Guttentag, S. H., Wade, K. C., Postle, A. D. & Ballard, P. L. Differentiation of
556 human pulmonary type II cells in vitro by glucocorticoid plus cAMP. *Am. J. Physiol. Lung Cell.*
557 *Mol. Physiol.* **283**, L940-51 (2002).
558 17. Nikolić, M. Z. *et al.* Human embryonic lung epithelial tips are multipotent progenitors that can
559 be expanded in vitro as long-term self-renewing organoids. *Elife* **6**, (2017).
560 18. Miller, A. J. *et al.* In Vitro Induction and In Vivo Engraftment of Lung Bud Tip Progenitor Cells
561 Derived from Human Pluripotent Stem Cells. *Stem Cell Reports* **10**, 101–119 (2018).
562 19. Lim, K. *et al.* Organoid modeling of human fetal lung alveolar development reveals mechanisms
563 of cell fate patterning and neonatal respiratory disease. *Cell Stem Cell* **30**, 20-37.e9 (2023).
564 20. He, P. *et al.* A human fetal lung cell atlas uncovers proximal-distal gradients of differentiation
565 and key regulators of epithelial fates. *Cell* **185**, 4841-4860.e25 (2022).
566 21. Brownfield, D. G. *et al.* Alveolar cell fate selection and lifelong maintenance of AT2 cells by
567 FGF signaling. *Nat. Commun.* **13**, 7137 (2022).
568 22. Alysandratos, K.-D. *et al.* Culture impact on the transcriptomic programs of primary and iPSC-
569 derived human alveolar type 2 cells. *JCI Insight* (2022) doi:10.1172/jci.insight.158937.
570 23. Burgess, C. L. *et al.* Generation of human alveolar epithelial type I cells from pluripotent stem
571 cells. *bioRxiv* 2023.01.19.524655 (2023) doi:10.1101/2023.01.19.524655.

572 24. Shiraishi, K. *et al.* Biophysical forces mediated by respiration maintain lung alveolar epithelial
573 cell fate. *Cell* **186**, 1478-1492.e15 (2023).
574 25. Menzies, S. A. *et al.* The sterol-responsive RNF145 E3 ubiquitin ligase mediates the degradation
575 of HMG-CoA reductase together with gp78 and Hrd1. *Elife* **7**, (2018).
576 26. Rosonina, E., Akhter, A., Dou, Y., Babu, J. & Sri Theivakadadcham, V. S. Regulation of
577 transcription factors by sumoylation. *Transcription* **8**, 220–231 (2017).
578 27. Chen, H. I. & Sudol, M. The WW domain of Yes-associated protein binds a proline-rich ligand
579 that differs from the consensus established for Src homology 3-binding modules. *Proc. Natl.*
580 *Acad. Sci. U. S. A.* **92**, 7819–7823 (1995).
581 28. Beers, M. F., Kim, C. Y., Dodia, C. & Fisher, A. B. Localization, synthesis, and processing of
582 surfactant protein SP-C in rat lung analyzed by epitope-specific antipeptide antibodies. *J. Biol.*
583 *Chem.* **269**, 20318–20328 (1994).
584 29. Kotorashvili, A., Russo, S. J., Mulugeta, S., Guttentag, S. & Beers, M. F. Anterograde transport
585 of surfactant protein C proprotein to distal processing compartments requires PPDY-mediated
586 association with Nedd4 ubiquitin ligases. *J. Biol. Chem.* **284**, 16667–16678 (2009).
587 30. Duerr, J. *et al.* Conditional deletion of Nedd4-2 in lung epithelial cells causes progressive
588 pulmonary fibrosis in adult mice. *Nat. Commun.* **11**, 2012 (2020).
589 31. Sun, D. *et al.* A functional genetic toolbox for human tissue-derived organoids. *Elife* **10**, (2021).
590 32. Lohr, N. J. *et al.* Human ITCH E3 ubiquitin ligase deficiency causes syndromic multisystem
591 autoimmune disease. *Am. J. Hum. Genet.* **86**, 447–453 (2010).
592 33. Aki, D. *et al.* The E3 ligases Itch and WWP2 cooperate to limit TH2 differentiation by enhancing
593 signaling through the TCR. *Nat. Immunol.* **19**, 766–775 (2018).
594 34. Wang, W.-J., Mulugeta, S., Russo, S. J. & Beers, M. F. Deletion of exon 4 from human surfactant
595 protein C results in aggresome formation and generation of a dominant negative. *J. Cell Sci.* **116**,
596 683–692 (2003).

597 35. Mulugeta, S., Nguyen, V., Russo, S. J., Muniswamy, M. & Beers, M. F. A surfactant protein C
598 precursor protein BRICHOS domain mutation causes endoplasmic reticulum stress, proteasome
599 dysfunction, and caspase 3 activation. *Am. J. Respir. Cell Mol. Biol.* **32**, 521–530 (2005).
600 36. Katzen, J. *et al.* An SFTPC BRICHOS mutant links epithelial ER stress and spontaneous lung
601 fibrosis. *JCI Insight* **4**, (2019).
602 37. Nureki, S.-I. *et al.* Expression of mutant Sftpc in murine alveolar epithelia drives spontaneous
603 lung fibrosis. *J. Clin. Invest.* **128**, 4008–4024 (2018).
604 38. Bridges, J. P., Wert, S. E., Nogee, L. M. & Weaver, T. E. Expression of a human surfactant
605 protein C mutation associated with interstitial lung disease disrupts lung development in
606 transgenic mice. *J. Biol. Chem.* **278**, 52739–52746 (2003).
607 39. Lawson, W. E. *et al.* Endoplasmic reticulum stress enhances fibrotic remodeling in the lungs.
608 *Proc. Natl. Acad. Sci. U. S. A.* **108**, 10562–10567 (2011).
609
610

611 **Methods and protocols**

612

613 Details of primary antibodies, expression plasmids, primers, guide RNA, and sample information are included
614 in supplementary table 1.

615

616 **Material Availability**

617 Human organoid lines used in the study are available from the Dr Emma L Rawlins (elr21@cam.ac.uk) with
618 a completed Materials Transfer Agreement.

619

620 **Mouse tissue**

621 6-10 week-old C57BL/6 mice were used for the ex vivo AT1 differentiation experiments. All procedures were
622 approved by the University of Cambridge Animal Welfare and Ethical Review Body and carried out under a
623 UK Home Office License (PPL: PP3176550) in accordance with the Animals (Scientific Procedures) Act 1986.
624 Mice were bred and maintained under specific-pathogen-free conditions at the Gurdon Institute of the
625 University of Cambridge.
626 Twelve-week old animals homozygous for a null allele of *Itch* ($Itch^{a18H/a18H}$, B6.C3H(101)-
627 In(2a;Itch)18H/LmatMmjax MMRRC stock #65285) have been previously described (Hustad et al., 1995;
628 Cattanach BM et al, 1987). For this line, the a^{18H} allele was backcrossed to C57BL/6J for 27 generations.
629 Therefore, age- and gender-matched C57BL/6J mice were used as controls ($Itch^{+/+}$) in the indicated
630 experiments. All mice were cared for in accordance with the National Institute of Health's Guide for the Care
631 and Use of Laboratory Animals (8th ed., Washington, DC: 2011) and the University of South Carolina's
632 Institutional Animal Care and Use Committee approved all experimental protocols.

633

634 **Human embryonic and fetal lung tissues**

635 Human embryonic and fetal lung tissue was provided from terminations of pregnancy from Cambridge
636 University Hospitals NHS Foundation Trust under permission from NHS Research Ethical Committee
637 (96/085) and the MRC/Wellcome Trust Human Developmental Biology Resource (London and Newcastle,
638 University College London (UCL) site REC reference: 18/LO/0822; Project 200591; www.hdbr.org). Sample
639 age ranged from 7-9[1] and from 16-22 weeks of gestation (post-conception weeks; pcw). Sample gestation was

640 determined by external physical appearance and measurements. Samples had no known genetic abnormalities.
641 Sample gender was unknown at the time of collection and was not determined. All collected samples were
642 included in the study.
643
644 **Derivation and *in vitro* culture of human alveolar type 2-like organoids**
645 Distal edges of 16~22 pcw human fetal lung tissue, typically measuring 0.5 cm x 1~3 cm, were sectioned and
646 fragmented into smaller pieces. Fragments were dissociated with 0.125 mg/ml Collagenase (Merck, C9891),
647 1 U/ml Dispase (Thermo Fisher Scientific, 17105041), and 0.1 U/µl DNase (Merck, D4527) in a rotating
648 incubator for 1 hr at 37°C. After rinsing in washing buffer containing 2% FBS in cold PBS the cells were
649 filtered through a 100 µm strainer. Cells were treated with RBC lysis buffer (BioLegend, 420301) at room
650 temperature for 5 min, rinsed and incubated with EpCAM (CD326) microbeads (Miltenyi Biotec; 130-061-
651 101) to isolate EpCAM+ epithelial cells containing mostly tip epithelial cells. These cells were embedded in
652 matrigel (Corning, 356231) and cultured in 24-well plates in alveolar type 2 differentiation medium (AT2
653 medium): Advanced DMEM/F12 supplemented with 1x GlutaMax, 1 mM HEPES and
654 Penicillin/Streptomycin, 1X B27 supplement (without Vitamin A), 1X N2 supplement, 1.25 mM N-
655 acetylcysteine, 50 nM Dexamethasone (Merck, D4902), 0.1 mM 8-Bromoadenosine 3'5'-cyclic
656 monophosphate (cAMP; Merck, B5386), 0.1 mM 3-Isobutyl-1-methylxanthine (IBMX; Merck, 15679), 50
657 µM DAPT (Merck, D5942), 100 ng/ml recombinant human FGF7 (PeproTech, 100-19), 3 µM CHIR99021
658 (Stem Cell Institute, University of Cambridge), 10 µM A83-01 (Tocris, 2939), and 10 µM Y-27632 (Merck,
659 688000). Medium was replaced every 2 days and cultures maintained for 2 weeks until the initial AT2 organoid
660 colonies formed in the matrigel droplet. Organoids were typically passaged at a 1 to 3 ratio weekly by gently
661 breaking into small fragments.
662 For SFTPC-GFP, or SCGB3A2-GFP[2] reporter cell isolation, the isolated tip progenitor cells or proximal
663 airway cells were immediately transduced and selected based on *SFTPC*-GFP or *SCGB3A2*-GFP with *EF1a*-
664 TagRFP reporter expression by flow cytometry, after 48 h of transduction and cultured for 3 weeks in the AT2
665 medium. As a control, proximal airway progenitors were immediately selected based on *SCGB3A2*-GFP after
666 48 h of transduction, and cultured in airway medium: Advanced DMEM/F12 medium supplemented with 1X
667 B27, 1X N2, 1.25 mM N-acetylcysteine, 100 ng/mL FGF10, 100 ng/mL FGF7, 50 nM Dexamethasone, 0.1
668 mM cAMP, 0.1 mM IBMX, and 10 µM Y-27632.

669

670 **Immortalised cell culture and cell line derivation**

671 HeLa cells were cultured in DMEM (Sigma-Aldrich, D6429) + 10% fetal bovine serum (FBS) (Sigma-
672 Aldrich). Plasmid DNA was introduced using liposomal transfection with FuGene 6 (Promega) or
673 lipofectamine LTX (ThermoFisher).

674 Clonal GFP-SFTPC-expressing HeLa cell lines were derived as previously described[3]. A pool stably
675 expressing Cas9 was generated by lentiviral transduction of the pHRSIN-Cas9 vector and selection of
676 transduced cells using hygromycin (2 µg/ml; Invitrogen 10687010).

677 For initial CRISPR screen validation, gene-specific deplete pools were obtained by transducing HeLas with
678 pKLV-pU6-esgRNA(modified BbsI)-pPGK-Puro2ABFP containing 3 gRNAs per gene and transduced cells
679 selected with puromycin (1 µg/ml; Alfa Aesar J61278). *ITCH* depleted clonal lines were subsequently derived
680 by single cell sorting into 96 well plates before expansion and screening by RT-qPCR. Experiments were
681 performed on a minimum of 3 clonal lines derived from different gRNAs to ensure findings did not reflect off-
682 target effects.

683 For ITCH rescue experiments, 4 silent mutations were introduced into the *ITCH* cDNA sequence in the region
684 of the gRNA by site-directed mutagenesis (GAA CGG CGG GTT GAC AAC ATG -> GAG CGG CGG GTA
685 GAT AAT ATG) before transfection to ensure the integrated CRISPR-Cas9 in the ITCH knockout cells did
686 not also edit the transiently transfected plasmid.

687 To determine the efficacy of candidate CRISPRi gRNAs, HeLas were transduced with pLenti-tetON-KRAB-
688 dCas9-DHFR-EF1a-TagRFP-2A-tet3G and sorted by FACS. Expression was induced with TMP and dox for
689 5 days before cells harvested for RNA and RT-qPCR.

690

691 **Alveolar type 1 (AT1) lineage differentiation of AT2 organoids *in vitro* and *ex vivo***

692 For *in vitro* AT1 differentiation, AT2 organoids were dissociated into single cells and 1 x 10^5 cells were
693 replated on matrigel-coated 12-well dishes and cultured either 1) in an AT1-promoting medium[4] containing
694 10% human serum for 2 weeks or 2) in medium[5] containing the LATS1 and 2 inhibitor LATS-IN-1 (10 mM,
695 Cambridge Bioscience, CAY36623) and in the absence of CHIR99021 for a week. Cells were analysed by RT-
696 qPCR and immunofluorescence.

697 AT1 lineage differentiation of AT2 organoids was performed in an *ex vivo* mouse lung explant. Prior to the *ex*
698 *vivo* culture of precision-cut lung slices (PCLS)[6], AT2 organoids expressing *SFTPC*-GFP+ and TagRFP+ were
699 dissociated into single cells, 2 x 10^5 cells mixed with 100 µl 50% matrigel and directly injected into each lung
700 lobe using an 18G needle. Mouse lung lobes were sectioned into 150 µm PCLS using a Leica VT1200s
701 vibratome. Following *ex vivo* culture in DMEM/F12 medium supplemented with 2% v/v penicillin-
702 streptomycin, 10% FBS and 1 mM cAMP for one week, the PCLS were subjected to immunofluorescence
703 analysis.
704
705 **Lentivirus production and viral transduction**
706 Lentivirus was produced using HEK293T cells. For pHRSIN and pKLV vectors (for the forward genetic
707 screen), 5 x 10^5 cells were plated in one well of a 6-well plate 24 hr before transfection with 0.67µg
708 pCMVR8.91 (Gag-Pol), 0.33µg pMD2G (VSV-G) and 1µg pHRSIN/pKLV (with gene of interest) and media
709 was changed the next day. Virus was collected after 48 hr and filtered through a 0.45µm filter. For pLenti
710 vectors for the CRISPRi experiments and generating SFTPC-GFP reporter line, 2 x 10^5 / 8 x 10^5 cells (<10kb
711 / >10kb plasmid, respectively) were plated into a 10cm dish 24 hr before transduction with 5/10µg plasmid of
712 interest, 3/6µg pPAX2, 2/3µg pMD2.G and 2/3µg pAdvantage and media was changed the next day. Virus was
713 collected after 48 hr and filtered through a 0.45 µm filter before being concentrated with Lenti-X (Takara bio)
714 (3:1 supernatant to lenti-X) overnight at 4°C, spun at 1,500 g for 45 min in a cold centrifuge and the pellet
715 resuspended such that virus was 100X concentrated.
716 Transduction of HeLa cells was typically achieved by adding 500 µl viral supernatant to 2 x 10^5 cells in a 6-
717 well plate, centrifuging at 600 x g for 1 hr and incubating overnight before refreshing the media. Antibiotic
718 selection was added 48 hr after transduction.
719
720 **Genetic manipulation of organoids**
721 To create transduced organoid lines, single-cell dissociated AT2 organoids were infected with lentivirus
722 overnight at 37°C then embedded into matrigel and cultured in the medium for another 48-72 before
723 fluorescence sorting to enrich for transduced cells. For the reporter system, pHAGE plasmids were modified
724 by insertion of EGFP or EF1a-promoter TagRFP (EF1a-TagRFP) cassettes into the human *SFTPC* promoter

725 (2.2 kb; chr8:22,433,535-22,435,769). For the HA-SFTPC lines, HA-SFTPC-WT or I73T were cloned into
726 pLenti-tetON-EF1a-tagRFP-2A-tet3G by Gibson assembly.
727 For CRISPRi, the organoids were initially transduced with doxycycline- inducible lentivirus[7] containing
728 dCAS9 protein fused with 5' KRAB and 3' DHFR, and EF1a-TagRFP vector Post-sorting, organoids were
729 expanded before being transduced with lentivirus harbouring U6 promoter driven guide RNAs and EF1a-
730 EGFP-CAAX, with the relevant guides[8]. For activation of the CRIPSRi system, doxycycline (2 µg/ml, Merck,
731 D9891) and trimethoprim (10 nmol/l, Merck, 92131) were added to the medium for 5 days. For rescue
732 experiments, doxycycline and trimethoprim were removed from the media for 14 days and organoids passaged
733 where necessary before harvesting. CRISPRi experiments were carried out in two biologically independent
734 lines.
735
736 **CRISPR screen**
737 The forward genetic screen was undertaken using a ubiquitome gRNA library consisting of approximately
738 1,119 genes with 10 guides per gene[9]. The Cas9 activity of the HeLa-Cas9 line was confirmed by transducing
739 with pKLV encoding β-2 microglobulin gRNA and assessing loss of MHC class I from the plasma membrane
740 by flow cytometry (with >80% loss considered acceptable). The amount of virus required for an MOI of 0.3
741 was determined by transducing $1x10^6$ cells with varying amounts (25-400 µl) lentivirus and assessing BFP
742 positivity by flow cytometry at 72 hr post transduction. For the screen, 20 million cells were transduced to
743 ensure 500-fold coverage and puromycin selection commenced at 48 hr post transduction. After 5 days of
744 selection, cells were harvested with 10mM EDTA and stained using the SFTPC BRICHOS domain antibody.
745 Cells most highly enriched for BRICHOS signal or GFP (approx. 1%) were collected; half were harvested for
746 genomic DNA extraction and half kept in culture for a further 7 days. This population underwent a further sort
747 and the BRICHOS or GFP enriched population harvested. Genomic DNA was extracted using a Qiagen
748 Puregene Core Kit (#1042601). Lentiviral gRNA inserts were amplified in a two-step PCR reaction as
749 previously described (Menzies et al, 2018), cleaned with AMPure XP magnetic beads (Beckman Coulter
750 A63881) and sequenced by MiniSeq (Illumina).
751
752 **Flow cytometry**

753 HeLa cells were detached using 10 mM EDTA and organoids dissociated to single cells before being washed
754 with PBS and centrifuged at 500 g for 3 min to pellet. Non-specific staining was blocked with 10% FBS in
755 PBS for 30 min then cells pelleted by centrifugation and incubated with primary antibody on ice for 30 min.
756 Following two rounds of washing with PBS by centrifugation, cells were incubated with AF647-conjugated
757 secondary antibodies for 30 min on ice, washed twice and filtered through 50 µm filters. Samples were
758 analysed on a Fortessa (BD bioscience) flow cytometer and further analysis undertaken using FlowJo software
759 (10.0.0).
760 Flow cytometric sorting of single-cell dissociated organoids transduced with fluorescent markers was
761 performed using a sorter (SH800S or BD FACSMelody) and analysed using FlowJo.
762
763 **Immunoblotting**
764 For immunoblotting, cells were subjected to triton lysis, SDS-PAGE electrophoresis, and immunoblotting as
765 previously described[10]. Membranes were incubated overnight with primary antibody at 4°C before washing
766 and incubating with secondary antibody (1:20,000 IRDye® conjugated, various) for 1 hour at room
767 temperature. Membranes were visualised using a Li-Cor Odyssey imaging system.
768
769 **Immunofluorescence staining**
770 For immunostaining of Hela cells, cells grown on coverslips were fixed with 4% PFA for 30 min, blocked with
771 10% FBS for 30 min then permeabilized for 30 min with 0.1% triton. Cells were incubated with primary
772 antibodies diluted in a blocking buffer overnight at 4°C. After washing with PBS and incubated with Alexa-
773 fluor conjugated secondary antibodies (1:500, various, Thermo Fisher) for 1 hr at room temperature before
774 staining with DAPI (1µg/ml, Merck, D9542) and mounting with Prolong Gold antifade (Invitrogen P36934).
775 For paraffin embedding (Figure 4), organoids were seeded onto 0.4 µm transwell inserts (Greiner Bio-One
776 662641) embedded in 50% matrigel. Organoids were fixed with 4% PFA for 30 min before the membrane was
777 released from the insert using a scalpel and embedded between layers of HistoGel (Epredia HG-4000-012)
778 before paraffin embedding. Samples were deparaffinised and rehydrated using sequential passes through
779 xylene (x3) then ethanol (100%, 70%, 50%, 0%) then antigen retrieval undertaken by boiling slides in sodium
780 citrate buffer (10mM sodium citrate, 0.05% tween 20 pH 6.0) for 10 minutes. Samples were blocked using 1%
781 BSA, 0.1% tween then incubated with primary antibodies overnight and Alexa-fluor conjugated secondary

782 antibodies (1:500, various, ThermoFisher) for 1 hr at room temperature before staining with DAPI, and
783 mounting with prolong gold antifade. Imaging was undertaken using a Zeiss LSM880 with airyscan and Zen
784 black software.
785 For whole-mount immunostaining of organoids and 2D AT1-like cells (Figures 1 and 2), the matrigel was
786 completely removed from the cultured organoids using cell recovery solution (Corning, 354253) then fixed
787 with 4% PFA for 30 min on ice. After rinsing in PBS washing solution containing 0.2% (v/v) Triton X-100
788 and 0.5% (w/v) BSA, the samples were incubated in permeabilization/blocking solution containing 0.2% (v/v)
789 Triton X-100, 1% (w/v) BSA, and 5% normal donkey serum (Stratech Scientific, 017-000-121-JIR) in PBS,
790 overnight at 4°C. Samples were then incubated with primary antibody at 4°C overnight, washed and incubated
791 with secondary antibody for 1 hour at room temperature. Nuclei were counterstained using DAPI. Prior to the
792 organoid imaging, step-wise treatments of 10%, 25%, 50%, and 97% (v/v) 2'−2'-thio-diethanol (TDE, Merck,
793 166782) were followed for clearing. Images were taken using a Leica SP8 confocal microscope or Zeiss
794 LSM880 with airyscan and Zen black software.
795 For lysosomal fluorescence, organoids incubated with Lysotracker at 37°C for 2 hr (Cell Signaling
796 Technologies, 8783S) and immediately imaged under a fluorescence microscope.
797
798 **Quantitative RT-PCR**
799 Total RNA was isolated using an RNeasy kit (Qiagen, 74004) including an optional DNase digestion step.
800 Typically 500 ng RNA was used as the starting template to create cDNA using a high capacity cDNA reverse
801 transcription kit (Applied Biosystems, 4368814) and heating samples to 25°C for 10 min, 37°C for 2 h and
802 85°C for 5 min. RT-qPCR was undertaken in 96 well plates using 4.5µl 1:10 cDNA and 10.5 µl of a master
803 mix containing (Sigma-Aldrich, S4438) or SYBR Green PCR Master Mix (Applied Biosystems, 4309155).
804 Primer sequences are listed in Supplementary Table 1. Plates were run on a BioRad RT PCR machine typically
805 using the following programme: 95°C 2 min, 40x (95°C for 30 sec, 55°C for 30 sec, 72°C for 30 sec), 95°C
806 for 30 sec.
807
808 **Bulk RNA-sequencing**
809 For AT2 organoid bulk RNA-sequencing, RNA libraries of four biological lines of AT2 organoids at early
810 (P1,4,6,7) and late (P12,13,16,17) passage were generated using an RNeasy kit (Qiagen, 74004) including the

811 optional DNAse digestion step. The quality of the RNA libraries was validated on Agilent 2200 Tapestation
812 before sequencing on an Illumina NovaSeq 6000 at Novogene (novogene.com). A comparison between the
813 RNA sequencing data of AT2 organoids and publicly available data of fetal organoid types and other alveolar
814 cell types was performed: fetal early tip progenitor organoids GSM5393370 and GSM5393371; fetal late tip
815 progenitor organoids[11] GSM5393372 and GSM5393373; PSC-iAT2s[12] GSM5578511, GSM5578512 and
816 GSM5578513; cultured adult AT2 cells[12] GSM5578508, GSM5578509 and GSM5578510; freshly isolated
817 adult AT2 cells[13] GSM2537127, GSM2537128 and GSM2537129. The raw RNA sequencing data was run by
818 a bioinformatics pipeline, nf-core/rnaseq[14]. A list of differentially expressed genes was extracted using the
819 counted reads and R package edgeR[15] version 3.40.2. GO biological processes term enrichment, KEGG
820 pathway, and gene set enrichment analysis were performed using DAVID[16] and R package fgsea[17] packages.
821 Sequencing data have been deposited at GEO: GSE237359.
822
823 **Electron microscopy**
824 Whole organoids were fixed with 2% PFA, 2.5% glutaraldehyde, 0.1 M cacodylate buffer, pH 7.4. Organoids
825 were secondarily fixed with 1% osmium tetroxide/1.5% potassium ferrocyanide and then incubated with 1%
826 tannic acid in 0.1 M cacodylate buffer to enhance membrane contrast. Organoids were washed with water
827 before being dehydrated using increasing percentages of ethanol (70,%, 90%, 100%). Samples were embedded
828 in beam capsules in CY212 Epoxy resin and resin cured overnight at 65°C. Ultrathin sections were cut using
829 a diamond knife mounted to a Reichart ultracut S ultramicrotome. Sections were collected onto piloform-
830 coated slot grids and stained using lead citrate. Sections were viewed on a FEI Tecnai transmission electron
831 microscope at a working voltage of 80 kV.
832
833 **Bioinformatic and statistical analysis**
834 Statistical analysis of CRISPR screen sequencing data was performed using MAGeK[18]. Of note, the calculated
835 significance of a gene is not necessarily directly proportional to its biological significance; relative gRNA
836 efficiency and lethal phenotypes generated from knockdowns may preclude enrichment of other genes of
837 functional relevance.

838 Data expressed as mean ± standard deviation (SD) or standard error of mean (SEM) from at least three
839 independent experiments. Each statistical test is described in the figure legends. Graphpad Prism software
840 (version 9.5.1) was used for statistical analysis and data visualisation.
841
842 **Code Availability**
843 No new code was generated for use in this manuscript. Any additional information required to re-run the code
844 and repeat the analyses reported can be requested from the corresponding authors.
845
846 **References**

847 1. Nikolić, M. Z. *et al.* Human embryonic lung epithelial tips are multipotent progenitors that can be
848 expanded in vitro as long-term self-renewing organoids. *Elife* **6**, (2017).
849 2. He, P. *et al.* A human fetal lung cell atlas uncovers proximal-distal gradients of differentiation and key
850 regulators of epithelial fates. *Cell* **185**, 4841–4860.e25 (2022).
851 3. Dickens, J. A. *et al.* Novel insights into surfactant protein C trafficking revealed through the study of a
852 pathogenic mutant. *Eur. Respir. J.* **59**, (2022).
853 4. Kadur Lakshminarasimha Murthy, P. *et al.* Human distal lung maps and lineage hierarchies reveal a
854 bipotent progenitor. *Nature* **604**, 111–119 (2022).
855 5. Burgess, C. L. *et al.* Generation of human alveolar epithelial type I cells from pluripotent stem cells.
856 *bioRxiv* (2023) doi:10.1101/2023.01.19.524655.
857 6. Rosales Gerpe, M. C. *et al.* Use of Precision-Cut Lung Slices as an Ex Vivo Tool for Evaluating Viruses
858 and Viral Vectors for Gene and Oncolytic Therapy. *Mol Ther Methods Clin Dev* **10**, 245–256 (2018).
859 7. Sun, D. *et al.* A functional genetic toolbox for human tissue-derived organoids. *Elife* **10**, (2021).
860 8. Ran, F. A. *et al.* Genome engineering using the CRISPR-Cas9 system. *Nat. Protoc.* **8**, 2281–2308 (2013).
861 9. Menzies, S. A. *et al.* The sterol-responsive RNF145 E3 ubiquitin ligase mediates the degradation of
862 HMG-CoA reductase together with gp78 and Hrd1. *Elife* **7**, (2018).
863 10. Malzer, E. *et al.* Coordinate regulation of eIF2α phosphorylation by PPP1R15 and GCN2 is required
864 during Drosophila development. *J. Cell Sci.* **126**, 1406–1415 (2013).
865 11. Lim, K. *et al.* Organoid modeling of human fetal lung alveolar development reveals mechanisms of cell

866 fate patterning and neonatal respiratory disease. *Cell Stem Cell* **30**, 20–37.e9 (2023).

867 12. Abo, K. M. *et al.* Air-liquid interface culture promotes maturation and allows environmental exposure of
868 pluripotent stem cell-derived alveolar epithelium. *JCI Insight* **7**, (2022).

869 13. Jacob, A. *et al.* Differentiation of Human Pluripotent Stem Cells into Functional Lung Alveolar Epithelial
870 Cells. *Cell Stem Cell* **21**, 472–488.e10 (2017).

871 14. Ewels, P. A. *et al.* The nf-core framework for community-curated bioinformatics pipelines. *Nat.*
872 *Biotechnol.* **38**, 276–278 (2020).

873 15. Robinson, M. D., McCarthy, D. J. & Smyth, G. K. edgeR: a Bioconductor package for differential
874 expression analysis of digital gene expression data. *Bioinformatics* **26**, 139–140 (2010).

875 16. Huang, D. W., Sherman, B. T. & Lempicki, R. A. Systematic and integrative analysis of large gene lists
876 using DAVID bioinformatics resources. *Nat. Protoc.* **4**, 44–57 (2009).

877 17. Korotkevich, G. *et al.* Fast gene set enrichment analysis. *bioRxiv* 060012 (2021) doi:10.1101/060012.

878 18. Li, W. *et al.* MAGeCK enables robust identification of essential genes from genome-scale CRISPR/Cas9
879 knockout screens. *Genome Biol.* **15**, 554 (2014).

880

881

Figure 1

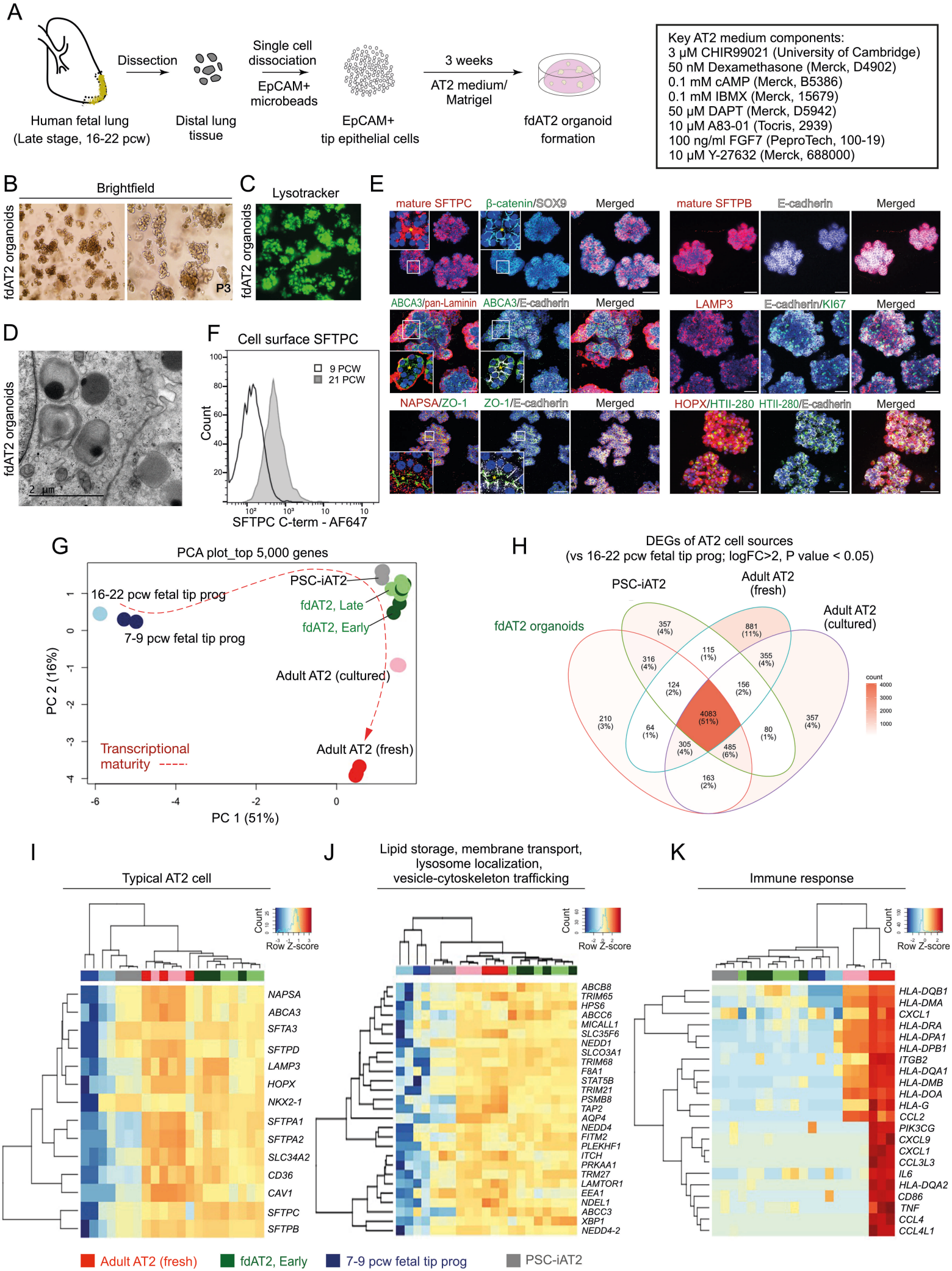
A
Human fetal lung
(Late stage, 16-22 pcw)
Dissection
Distal lung tissue
Single cell dissociation
EpCAM+ microbeads
EpCAM+ tip epithelial cells
3 weeks
AT2 medium/ Matrigel
fdAT2 organoid formation
Key AT2 medium components:
3 μM CHIR99021 (University of Cambridge)
50 nM Dexamethasone (Merck, D4902)
0.1 mM cAMP (Merck, B5386)
0.1 mM IBMX (Merck, 15679)
50 μM DAPT (Merck, D5942)
10 μM A83-01 (Tocris, 2939)
100 ng/ml FGF7 (PeproTech, 100-19)
10 μM Y-27632 (Merck, 688000)
B
Brightfield
fdAT2 organoids
P3
C
Lysotracker
fdAT2 organoids
D
fdAT2 organoids
2 μm
E
mature SFTPC
β-catenin/SOX9
Merged
mature SFTPB
E-cadherin
Merged
ABCA3/pan-Laminin
ABCA3/E-cadherin
Merged
LAMP3
E-cadherin/KI67
Merged
NAPSA/ZO-1
ZO-1/E-cadherin
Merged
HOPX/HTII-280
HTII-280/E-cadherin
Merged
F
Cell surface SFTPC
9 PCW
21 PCW
Count
SFTPC C-term - AF647
G
PCA plot_top 5,000 genes
16-22 pcw fetal tip prog
7-9 pcw fetal tip prog
PSC-iAT2
fdAT2, Late
fdAT2, Early
Adult AT2 (cultured)
Adult AT2 (fresh)
Transcriptional maturity
PC 2 (16%)
PC 1 (51%)
H
DEGs of AT2 cell sources
(vs 16-22 pcw fetal tip prog; logFC>2, P value < 0.05)
PSC-iAT2
Adult AT2 (fresh)
Adult AT2 (cultured)
fdAT2 organoids
count
I
Typical AT2 cell
Count
Row Z-score
NAPSA
ABCA3
SFTA3
SFTPD
LAMP3
HOPX
NKX2-1
SFTPA1
SFTPA2
SLC34A2
CD36
CAV1
SFTPC
SFTPB
J
Lipid storage, membrane transport, lysosome localization, vesicle-cytoskeleton trafficking
Count
Row Z-score
ABCB8
TRIM65
HPS6
ABCC6
MICALL1
SLC35F6
NEDD1
SLCO3A1
TRIM68
F8A1
STAT5B
TRIM21
PSMB8
TAP2
AQP4
NEDD4
FITM2
PLEKHF1
ITCH
PRKAA1
TRM27
LAMTOR1
EEA1
NDEL1
ABCC3
XBP1
NEDD4-2
K
Immune response
Count
Row Z-score
HLA-DQB1
HLA-DMA
CXCL1
HLA-DRA
HLA-DPA1
HLA-DPB1
ITGB2
HLA-DQA1
HLA-DMB
HLA-DOA
HLA-G
CCL2
PIK3CG
CXCL9
CXCL1
CCL3L3
IL6
HLA-DQA2
CD86
TNF
CCL4
CCL4L1
Adult AT2 (fresh)
Adult AT2 (cultured)
fdAT2, Early
fdAT2, Late
7-9 pcw fetal tip prog
16-22 pcw fetal late tip prog
PSC-iAT2

Figure 2

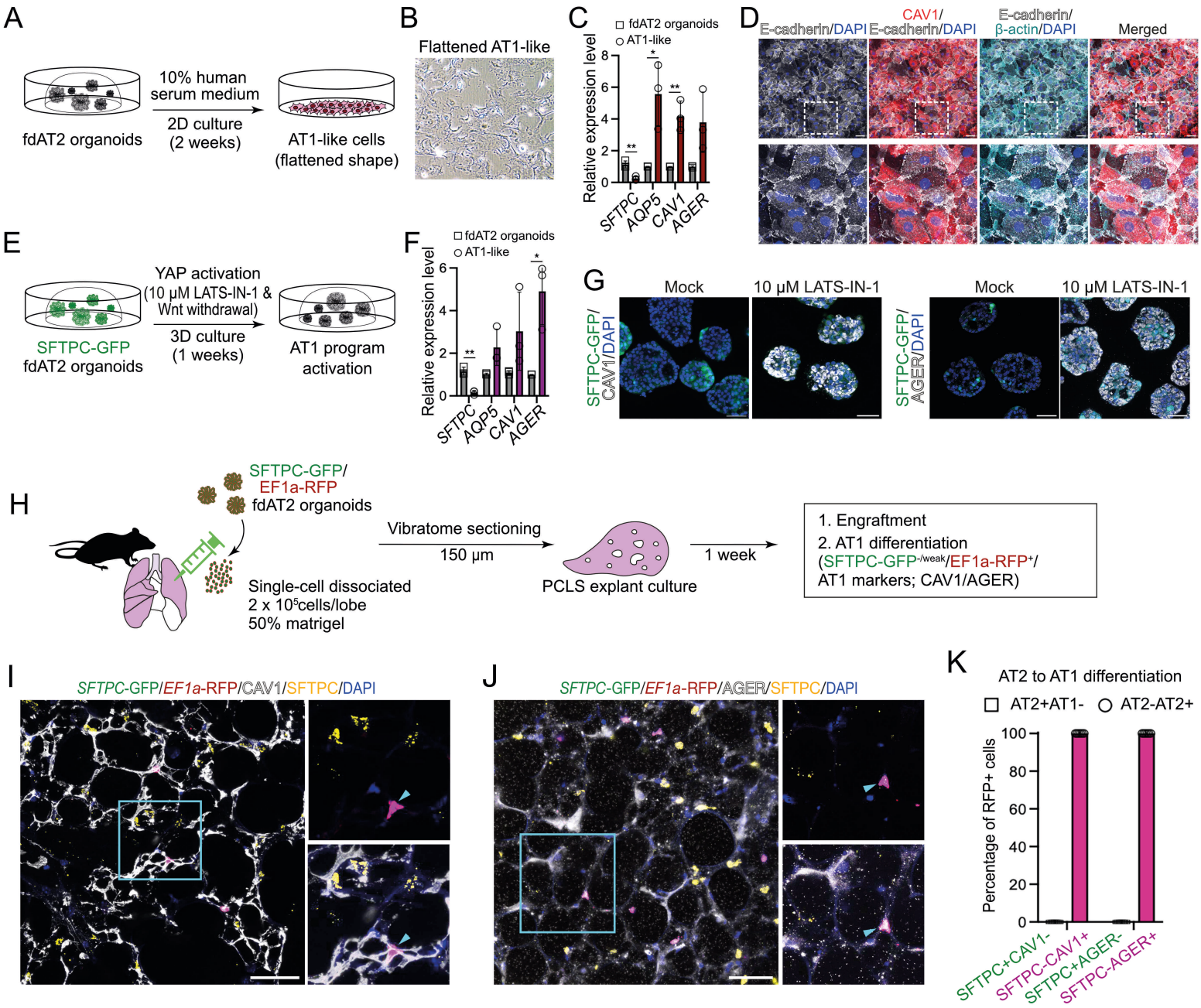
A
10% human serum medium
2D culture (2 weeks)
fdAT2 organoids
AT1-like cells (flattened shape)
B
Flattened AT1-like
C
fdAT2 organoids
AT1-like
Relative expression level
SFTPC
AQP5
CAV1
AGER
D
E-cadherin/DAPI
CAV1/ E-cadherin/DAPI
E-cadherin/ β-actin/DAPI
Merged
E
YAP activation (10 μM LATS-IN-1 & Wnt withdrawal)
3D culture (1 weeks)
SFTPC-GFP fdAT2 organoids
AT1 program activation
F
fdAT2 organoids
AT1-like
Relative expression level
SFTPC
AQP5
CAV1
AGER
G
Mock
10 μM LATS-IN-1
SFTPC-GFP/ CAV1/DAPI
SFTPC-GFP/ AGER/DAPI
H
SFTPC-GFP/ EF1a-RFP fdAT2 organoids
Single-cell dissociated
2 x 10⁵cells/lobe
50% matrigel
Vibratome sectioning
150 μm
PCLS explant culture
1 week
1. Engraftment
2. AT1 differentiation
(SFTPC-GFP-/weak/EF1a-RFP+/
AT1 markers; CAV1/AGER)
I
SFTPC-GFP/EF1a-RFP/CAV1/SFTPC/DAPI
J
SFTPC-GFP/EF1a-RFP/AGER/SFTPC/DAPI
K
AT2 to AT1 differentiation
AT2+AT1-
AT2-AT2+
Percentage of RFP+ cells
SFTPC+CAV1-
SFTPC-CAV1+
SFTPC+AGER-
SFTPC-AGER+

Figure 3

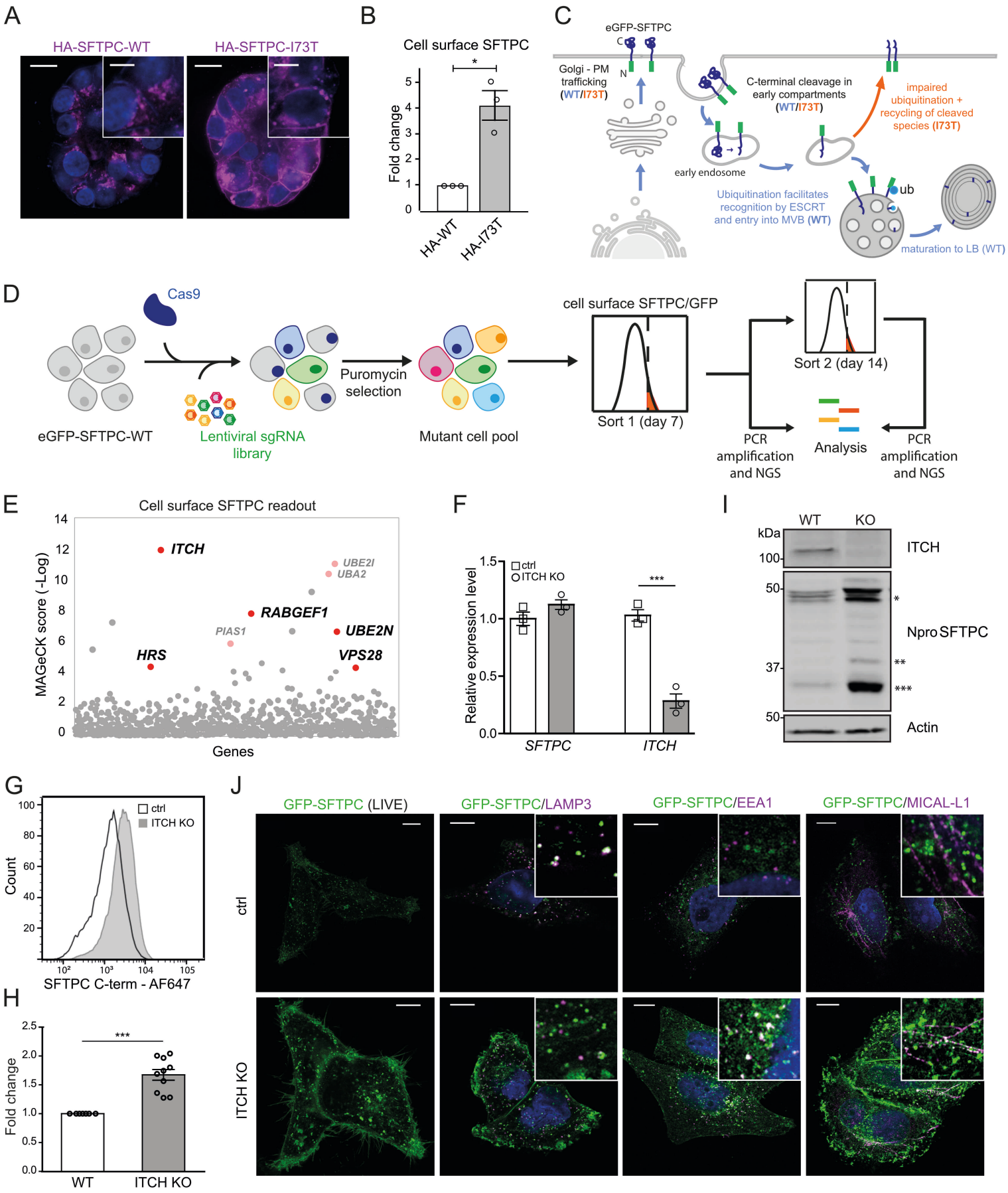
A
HA-SFTPC-WT
HA-SFTPC-I73T
B
Cell surface SFTPC
Fold change
HA-WT
HA-I73T
C
eGFP-SFTPC
Golgi - PM trafficking (WT/I73T)
C-terminal cleavage in early compartments (WT/I73T)
impaired ubiquitination + recycling of cleaved species (I73T)
early endosome
Ubiquitination facilitates recognition by ESCRT and entry into MVB (WT)
ub
maturation to LB (WT)
D
Cas9
eGFP-SFTPC-WT
Lentiviral sgRNA library
Puromycin selection
Mutant cell pool
cell surface SFTPC/GFP
Sort 1 (day 7)
Sort 2 (day 14)
PCR amplification and NGS
Analysis
PCR amplification and NGS
E
Cell surface SFTPC readout
MAGeCK score (-Log)
ITCH
UBE2I
UBA2
RABGEF1
PIAS1
UBE2N
HRS
VPS28
Genes
F
ctrl
ITCH KO
Relative expression level
SFTPC
ITCH
I
WT
KO
kDa
ITCH
Npro SFTPC
Actin
G
ctrl
ITCH KO
Count
SFTPC C-term - AF647
H
Fold change
WT
ITCH KO
J
GFP-SFTPC (LIVE)
GFP-SFTPC/LAMP3
GFP-SFTPC/EEA1
GFP-SFTPC/MICAL-L1
ctrl
ITCH KO

Figure 4

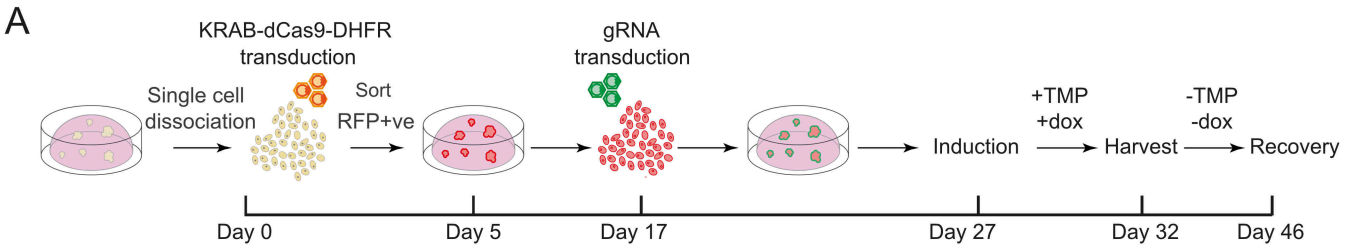
A
KRAB-dCas9-DHFR transduction
Single cell dissociation
Sort RFP+ve
gRNA transduction
Induction
+TMP +dox
Harvest
-TMP -dox
Recovery
Day 0
Day 5
Day 17
Day 27
Day 32
Day 46

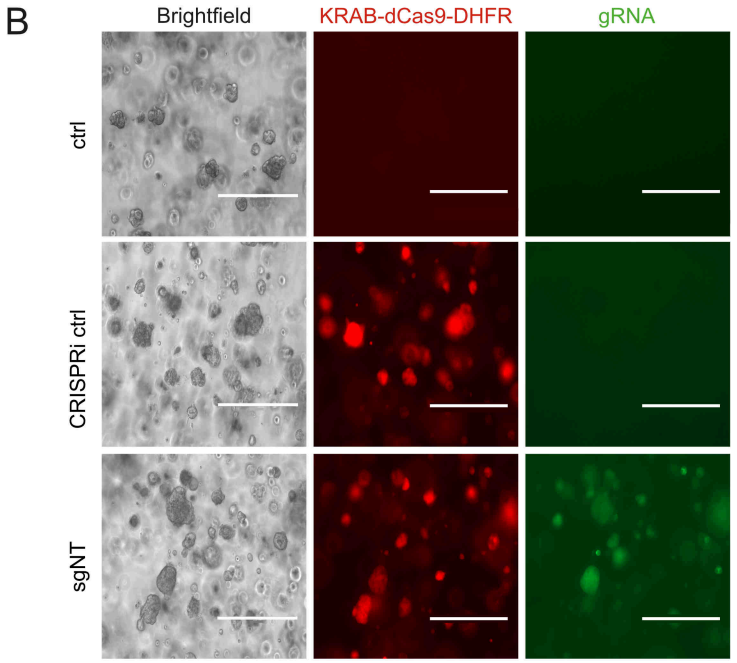
B
Brightfield
KRAB-dCas9-DHFR
gRNA
ctrl
CRISPRi ctrl
sgNT

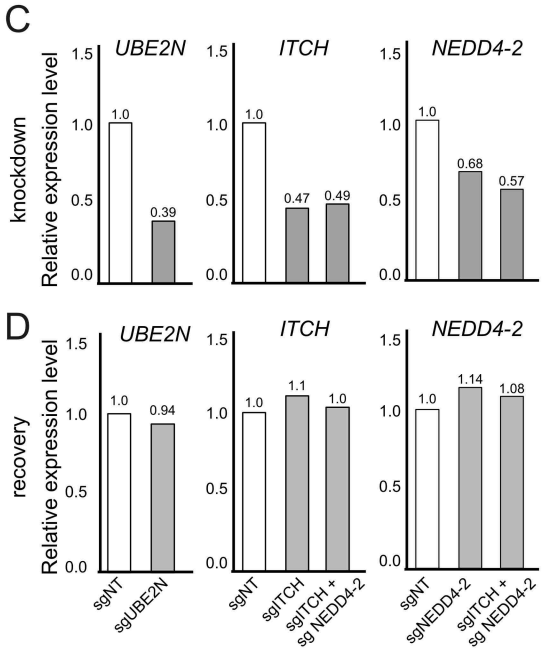
C
knockdown
Relative expression level
UBE2N
ITCH
NEDD4-2
1.0
0.39
1.0
0.47
0.49
1.0
0.68
0.57
D
recovery
Relative expression level
UBE2N
ITCH
NEDD4-2
1.0
0.94
1.0
1.1
1.0
1.0
1.14
1.08
sgNT
sgUBE2N
sgITCH
sgITCH + sg NEDD4-2
sgNEDD4-2

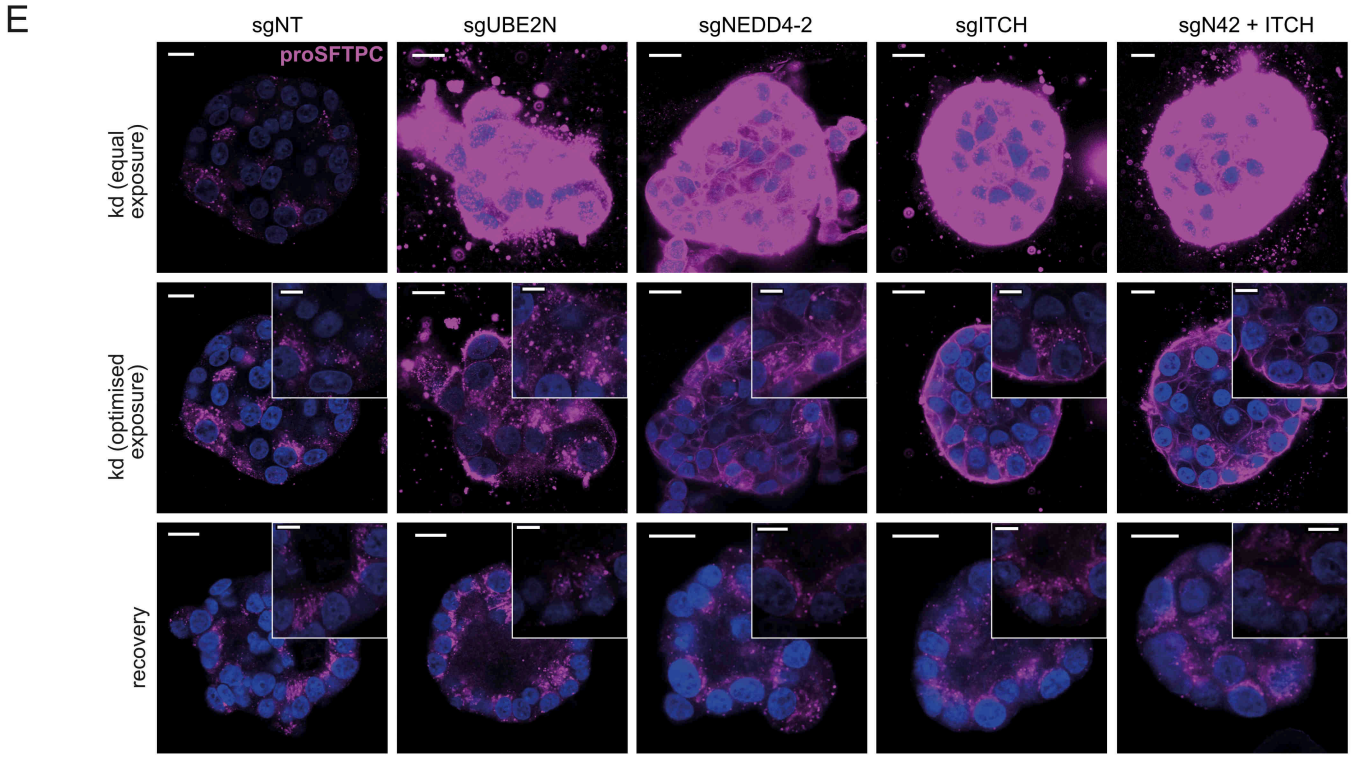
E
sgNT
sgUBE2N
sgNEDD4-2
sgITCH
sgN42 + ITCH
proSFTPC
kd (equal exposure)
kd (optimised exposure)
recovery

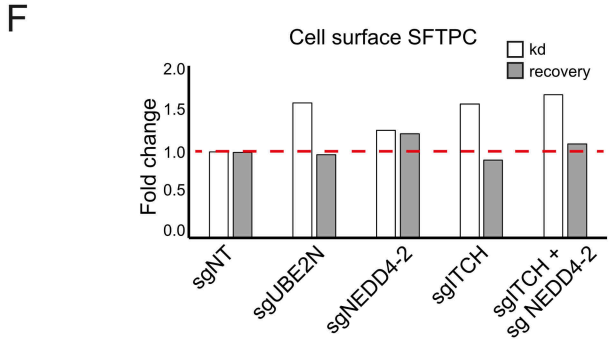
F
Cell surface SFTPC
kd
recovery
Fold change
2.0
1.5
1.0
0.5
0.0
sgNT
sgUBE2N
sgNEDD4-2
sgITCH
sgITCH + sg NEDD4-2

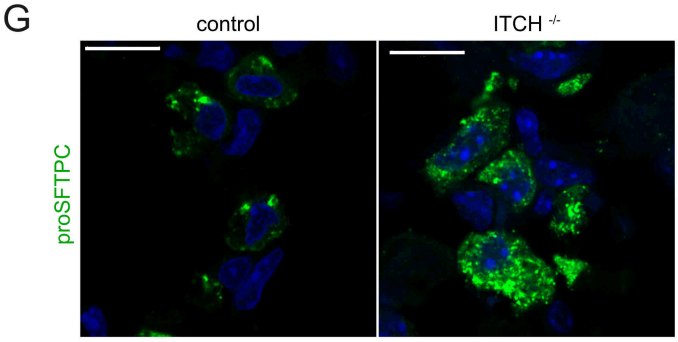
G
control
ITCH -/-
proSFTPC

Extended Data Figure 1

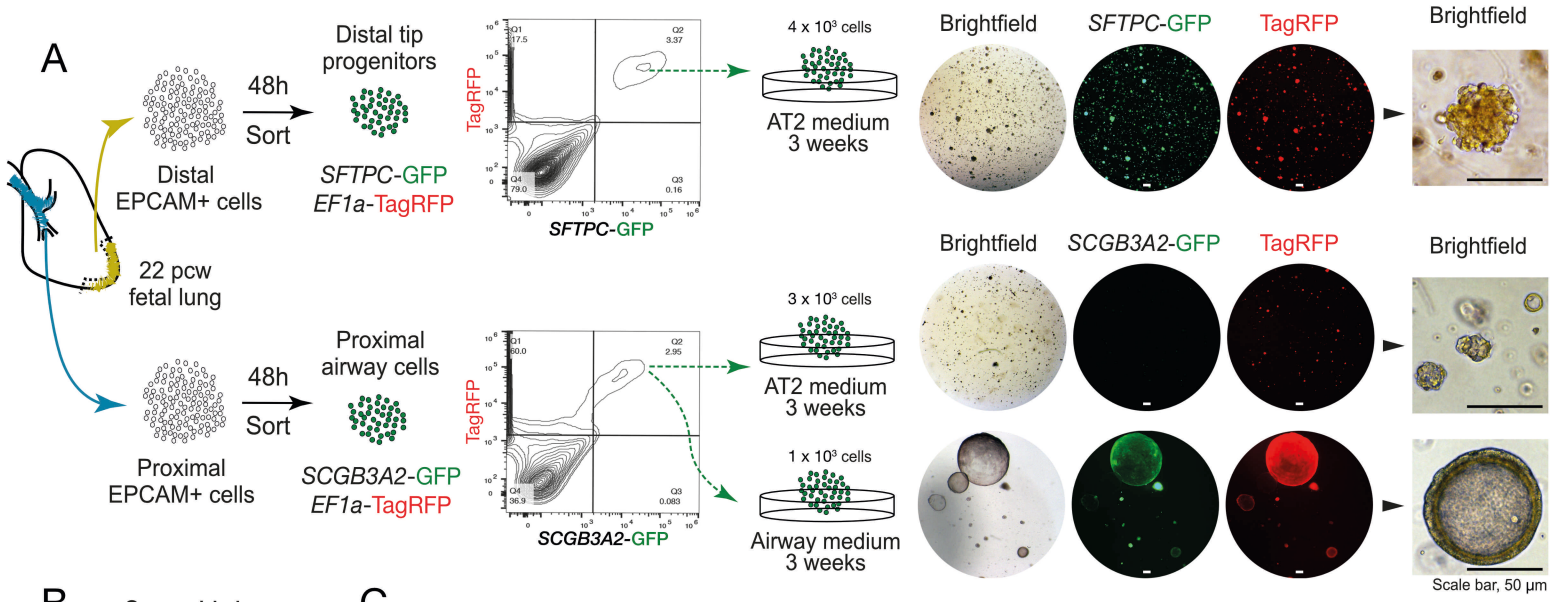

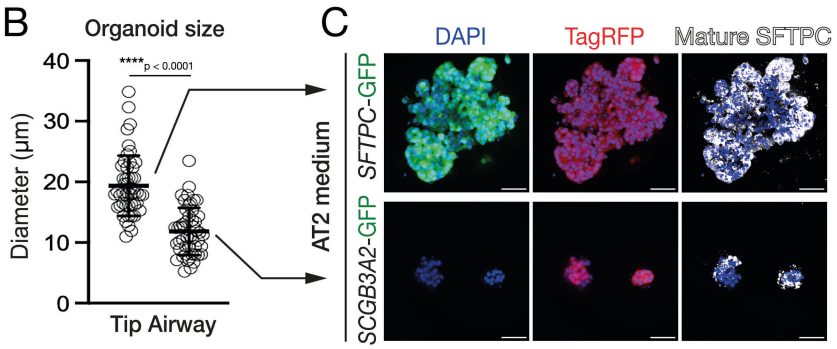

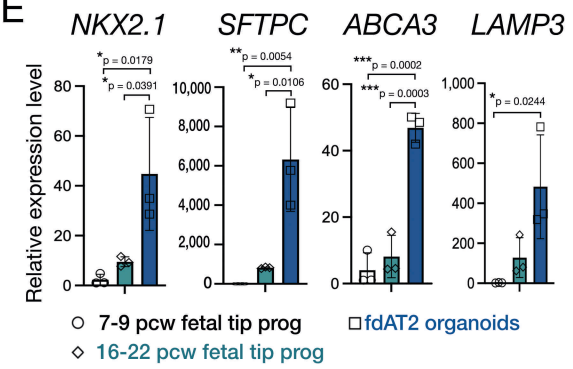

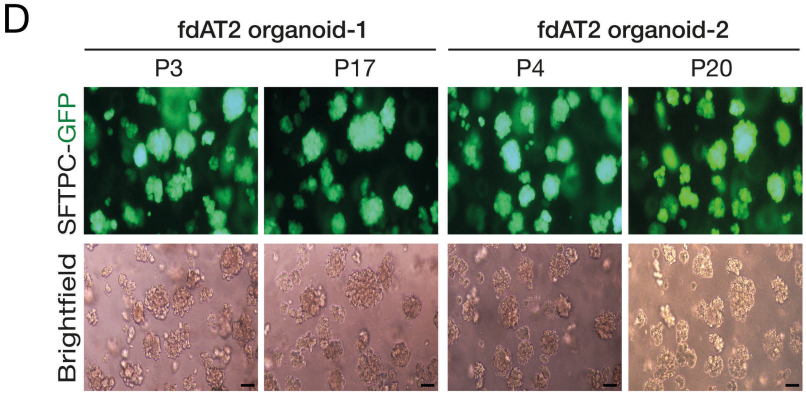

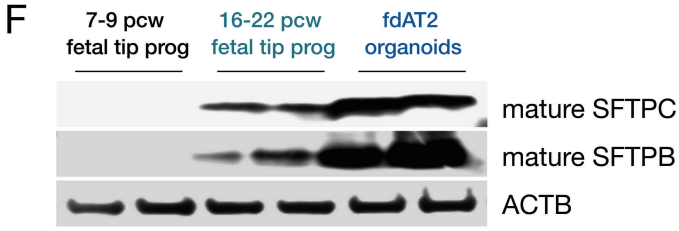

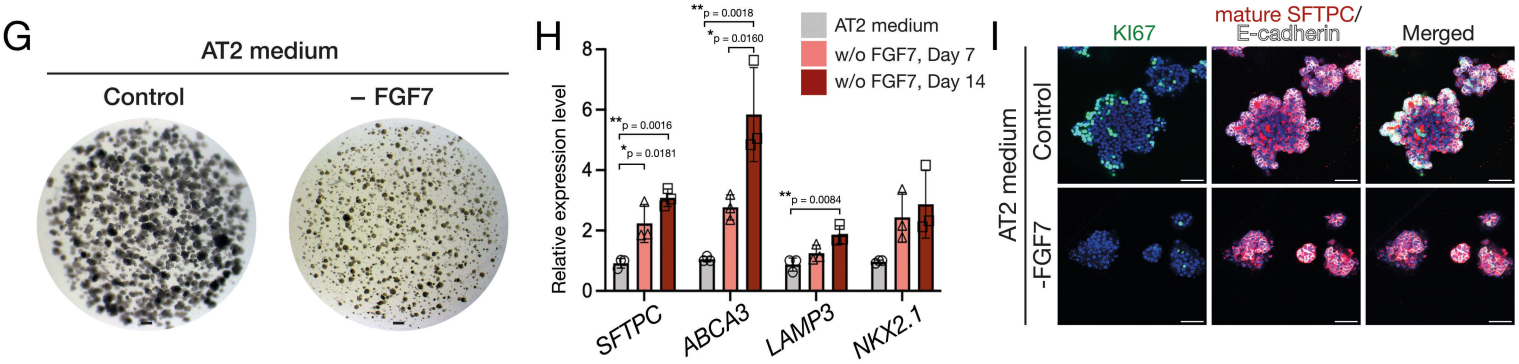

Extended Data Figure 2

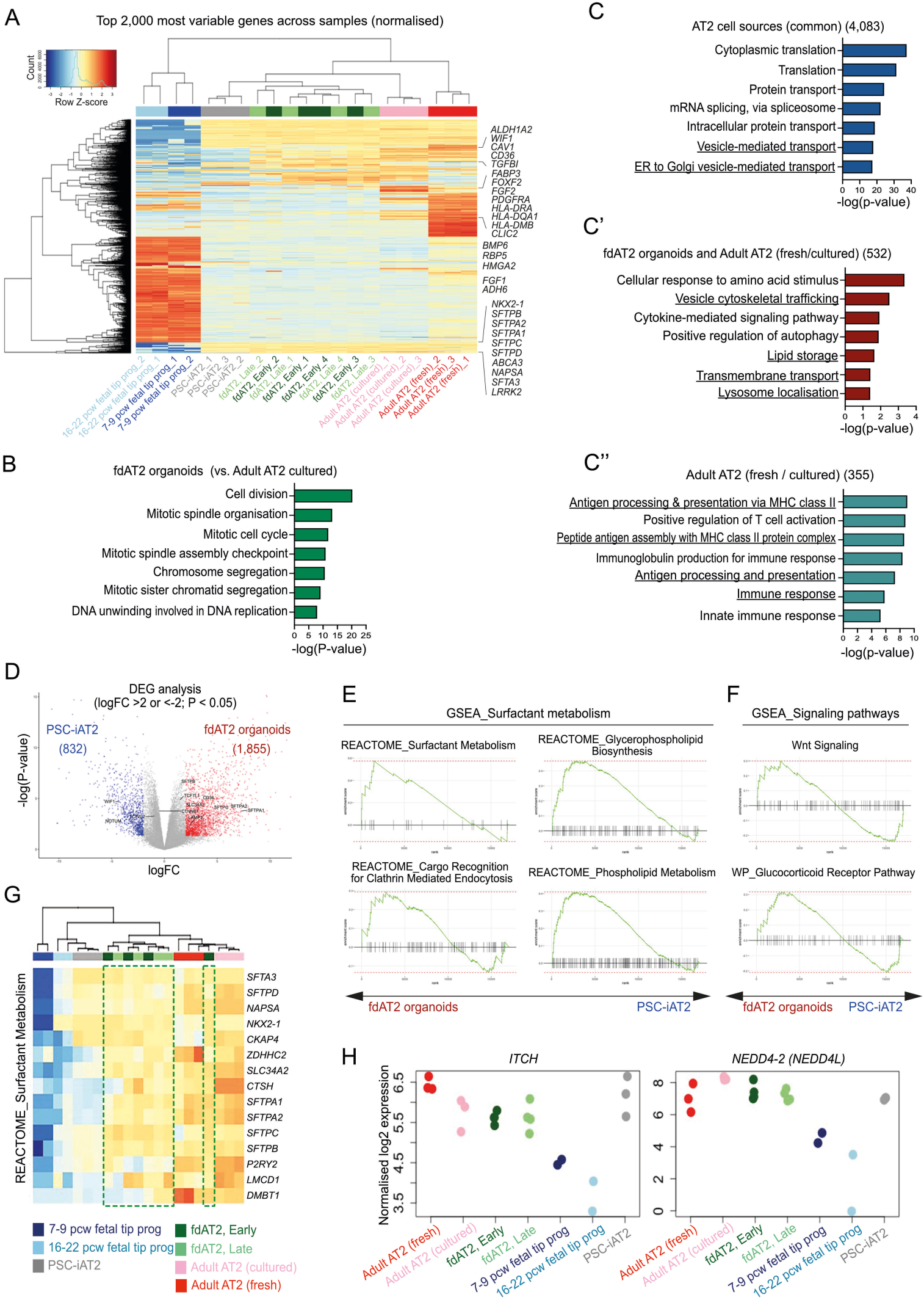

Extended Data Figure 3

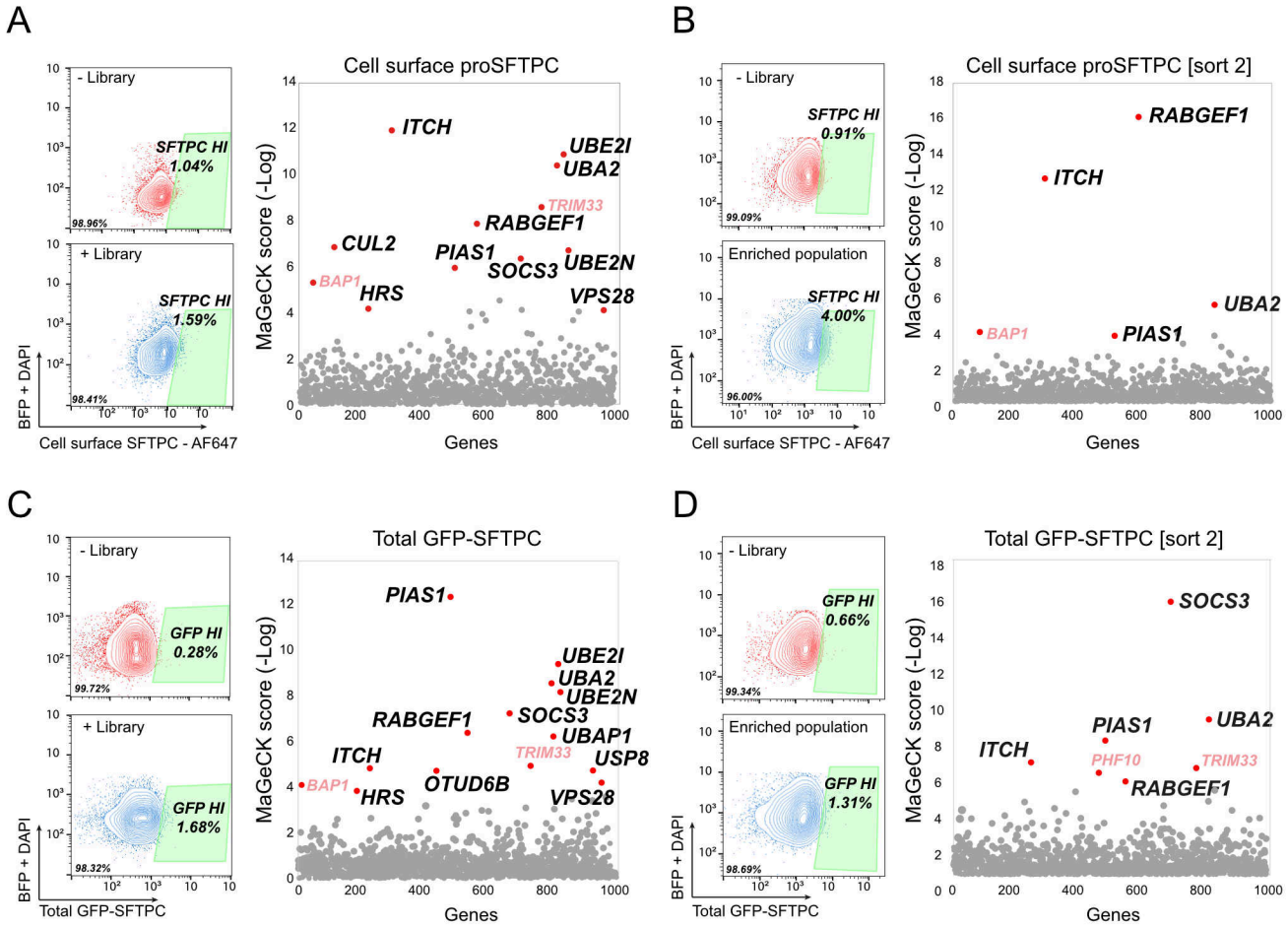

Extended Data Figure 4

A

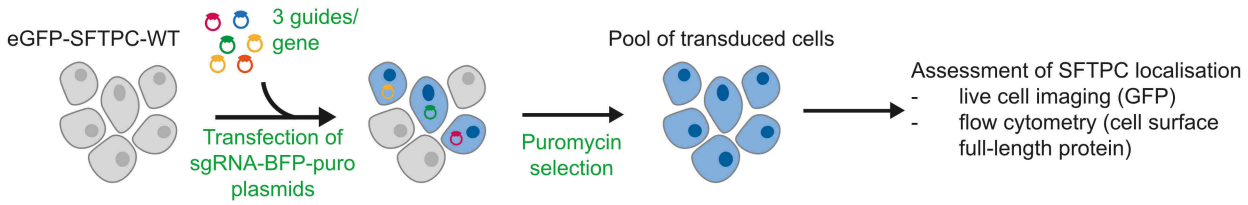

B

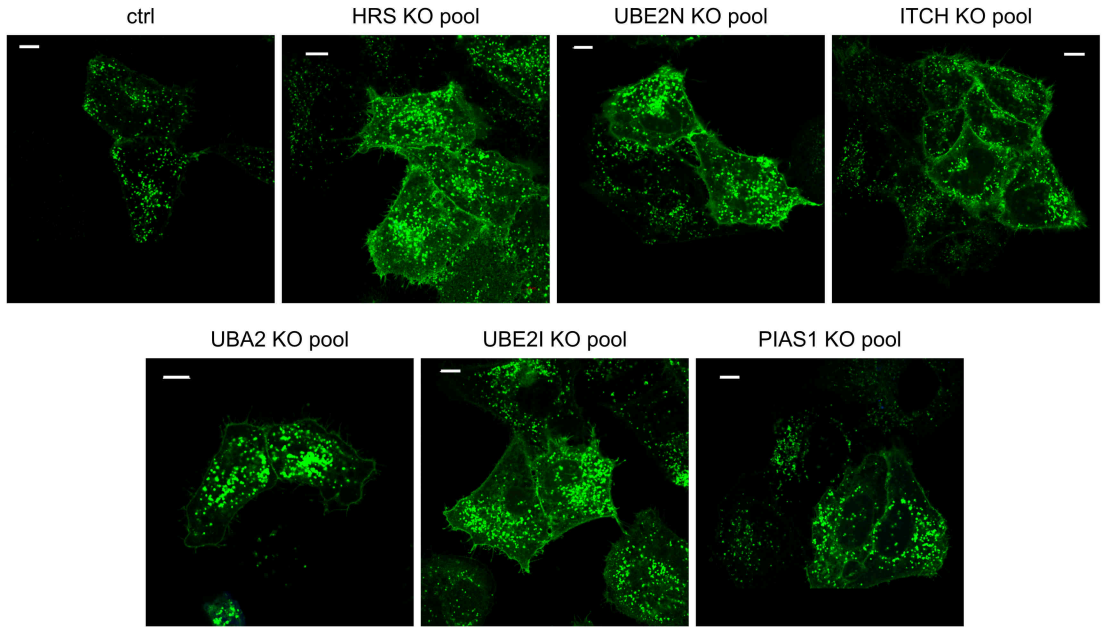

C

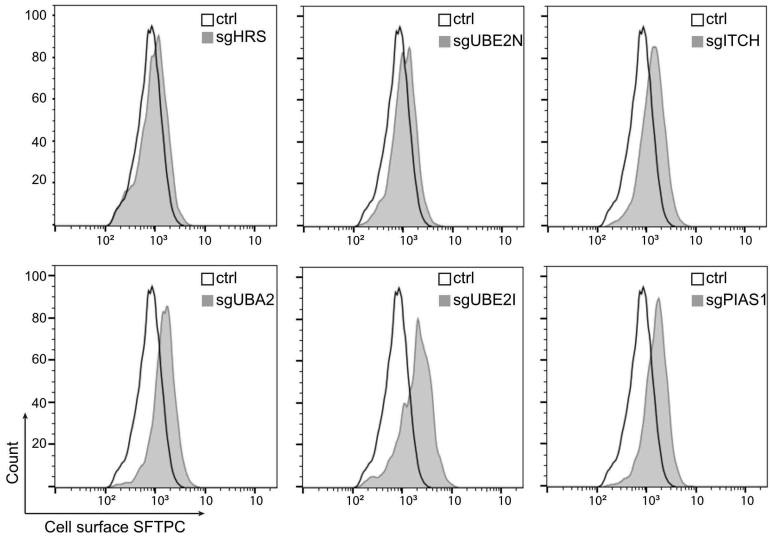

D

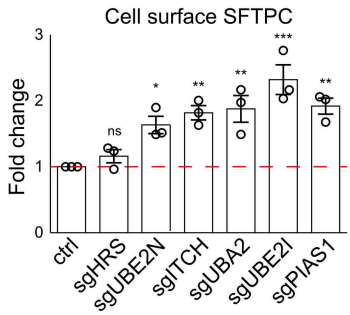

E

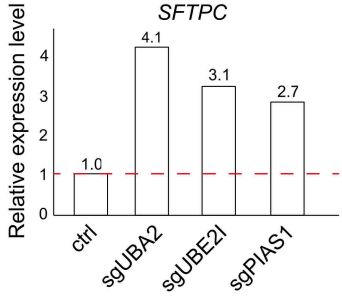

Extended Data Figure 5

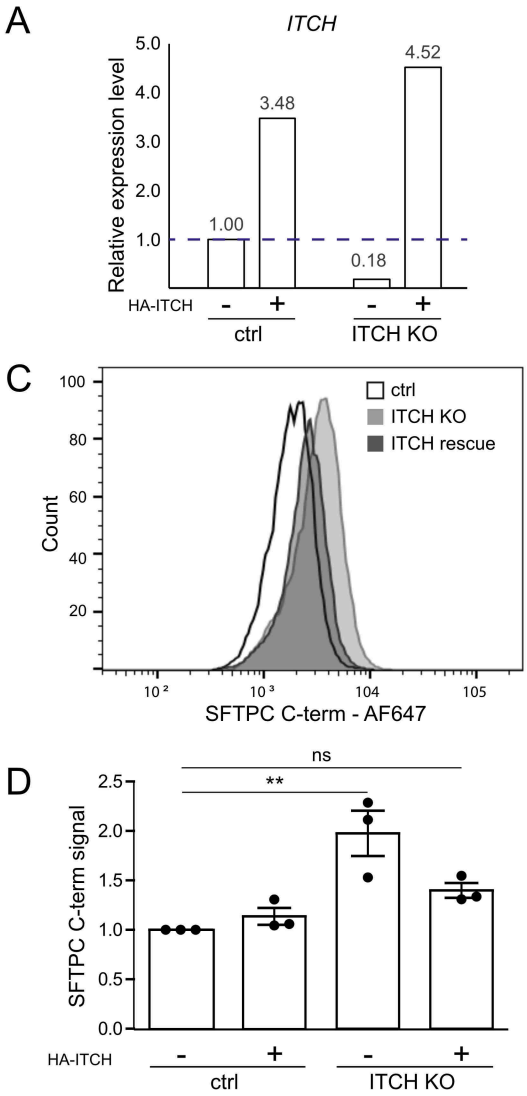

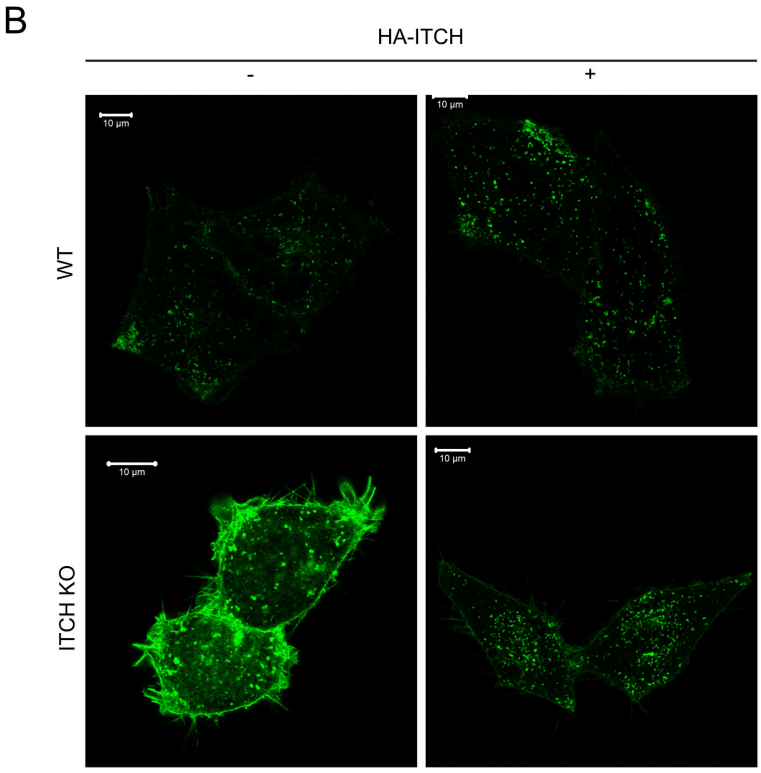
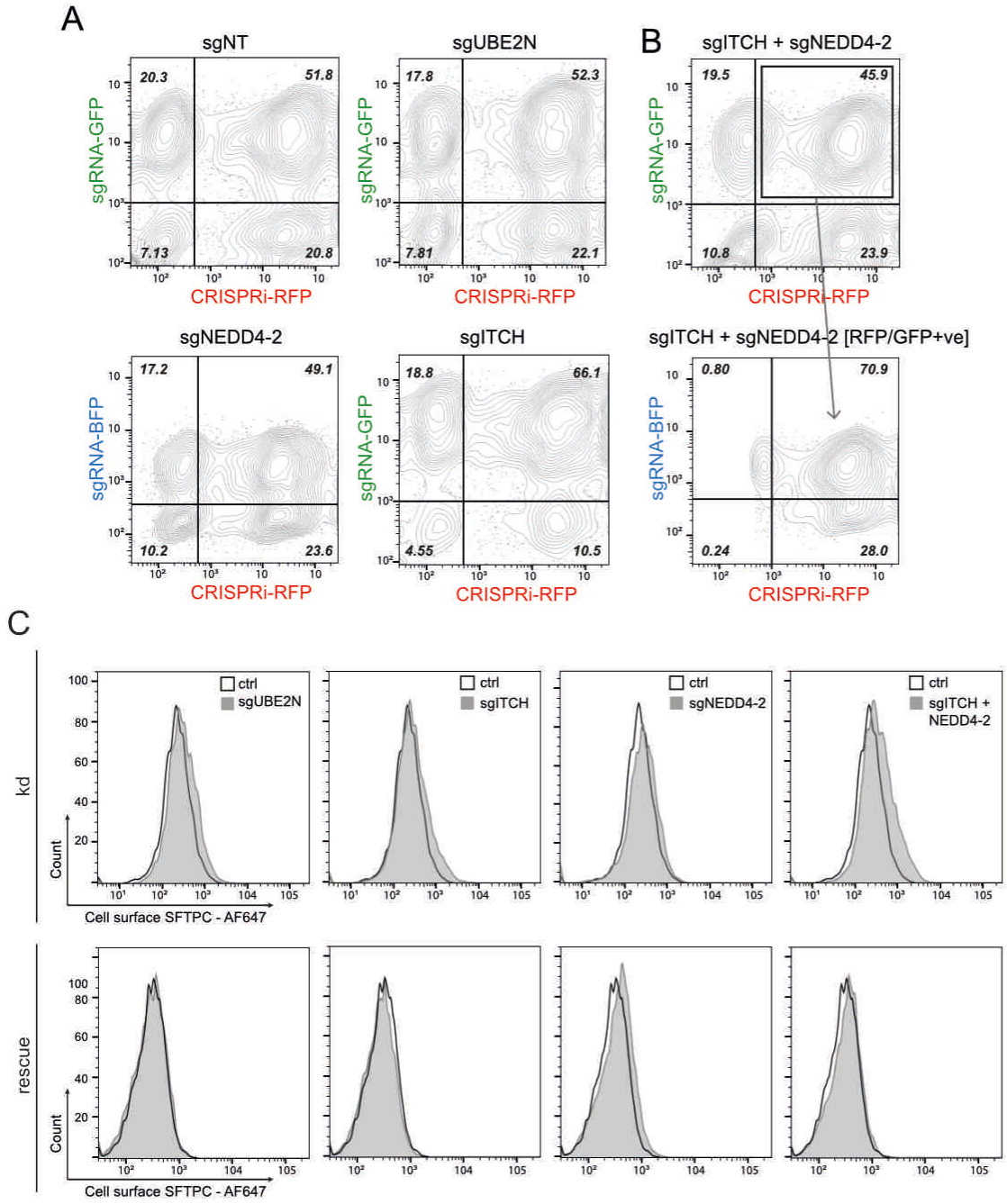
Extended Data Figure 6